Gemma

Sandia National Laboratories

SAND2020-1403C

A Sandia National Laboratories Electromagnetic Code for Heterogeneous Computer Architectures

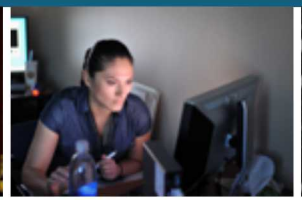

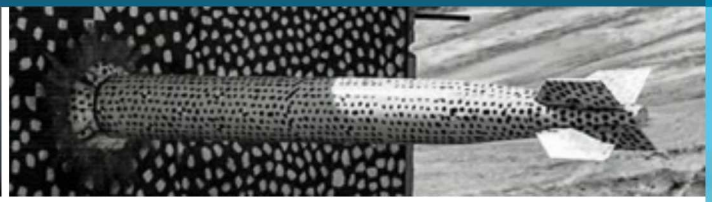

BY

Brian Zinser, Samuel Blake, Robert Pfeiffer, Andy Huang, John Himbele, Brian Freno, Vinh Dang, Joseph Kotulski, Sivasankaran Rajamanickam, William Johnson, Salvatore Campione, and William Langston

U.S. DEPARTMENT OF ENERGY NNSA

Sandia National Laboratories is a multimission laboratory managed and operated by National Technology and Engineering Solutions of Sandia LLC, a wholly owned subsidiary of Honeywell International Inc. for the U.S. Department of Energy's National Nuclear Security Administration under contract DE-NA0003525.

Capability and Performance on Next-Generation Hardware

eiger
FORTRAN
MPI Paradigm

- MPI inter- and intranode parallelism
- High processor clock speed
- High memory per processor

Gemma
Heterogenous
Paradigm

- MPI internode parallelism
- Threading intranode parallelism
- Low processor clock speed
- Low memory per processor

Ideal Development:

- Writing architecture independent source code
- Using multicore technology efficiently

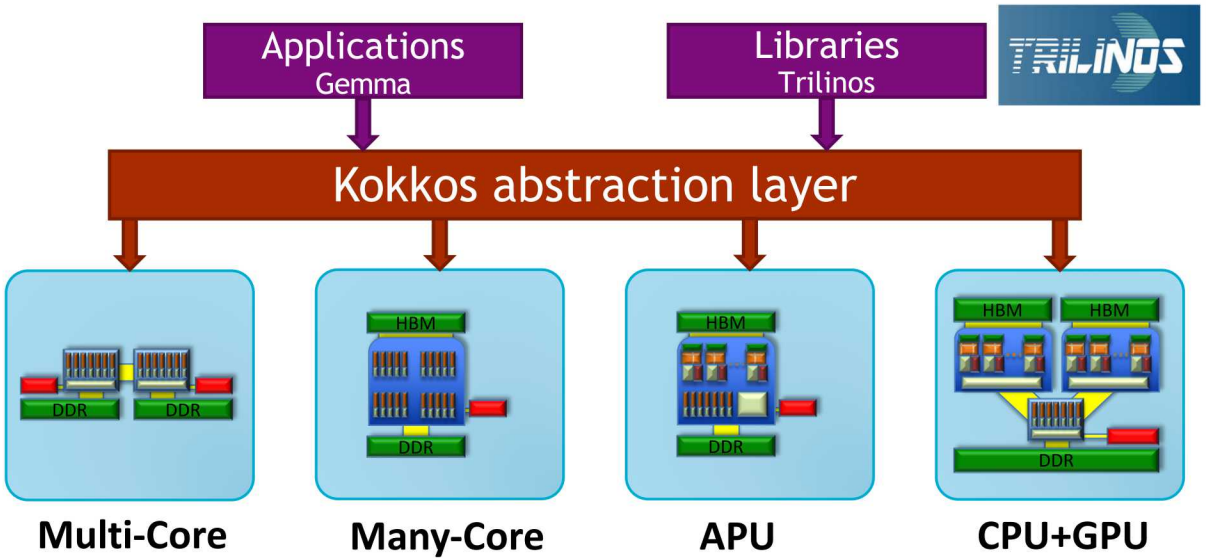

H. C. Edwards, C. R. Trott, and D. Sunderland, "Kokkos: Enabling manycore performance portability through polymorphic memory access patterns," *Journal of Parallel and Distributed Computing*, 74 (2014), pp. 3202-3216.

Outline

- Overview of Method of Moments
- Radar cross section use case and how it relates to our work
- Field levels near an object and some complications
- Primary use case: Coupling into high quality factor cavities

Method of Moments

Method of Moments (MoM) brief overview

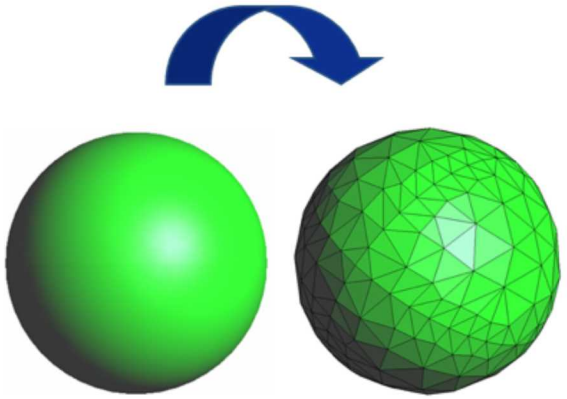

Through the equivalence principle, we consider the current on an objects boundary instead of the field around and inside the object. For electric field $\boldsymbol{E}$, magnetic field $\boldsymbol{H}$, electric current $\boldsymbol{J}$, and magnetic current $\boldsymbol{M}$,

$$\boldsymbol{E} = -i\omega\mu(\mathcal{L}\boldsymbol{J}) - (\mathcal{K}\boldsymbol{M})$$

$$\boldsymbol{H} = -i\omega\epsilon(\mathcal{L}\boldsymbol{M}) - (\mathcal{K}\boldsymbol{J})$$

$$\mathcal{L}\boldsymbol{X} = [1 + \frac{1}{k^2}\nabla\nabla\cdot]\int G(\boldsymbol{r},\boldsymbol{r}')\boldsymbol{X}(\boldsymbol{r}')d\boldsymbol{r}'$$

$$\mathcal{K}\boldsymbol{X} = \nabla\times\int G(\boldsymbol{r},\boldsymbol{r}')\boldsymbol{X}(\boldsymbol{r}')d\boldsymbol{r}'$$

$$G(r) = \frac{e^{-ikr}}{4\pi r}, \mathrm{r} = |\boldsymbol{r} - \boldsymbol{r}'|$$

Taking the first equation, but leaving off $\boldsymbol{M}$, gives the electric field integral equation (EFIE). Representing $\boldsymbol{J}$ with a basis $\boldsymbol{f}_n$, testing with a function $\boldsymbol{f}_m$ from the set of basis functions, and moving the derivatives off G, its discrete form Z is

$$Z_{m,n} = \int_{f_m}\int_{f_n}\left[i\omega\mu_l\boldsymbol{f}_m\cdot\boldsymbol{f}_n - \frac{i}{\omega\epsilon_l}\nabla\cdot\boldsymbol{f}_m\nabla'\cdot\boldsymbol{f}_n\right]\frac{e^{-ikr}}{4\pi r}$$

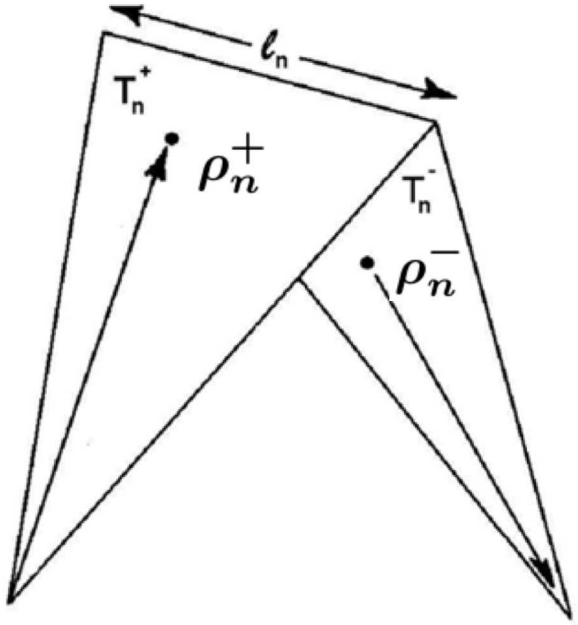

$$\mathbf{f_n}(\mathbf{r}) = \begin{cases} \frac{\ell_n}{2A_n^+}\boldsymbol{\rho_n^+} & \mathbf{r}\in T_n^+ \\ \frac{\ell_n}{2A_n^-}\boldsymbol{\rho_n^-} & \mathbf{r}\in T_n^- \\ \mathbf{0} & \text{otherwise} \end{cases}$$

Convergence and scaling for a sphere

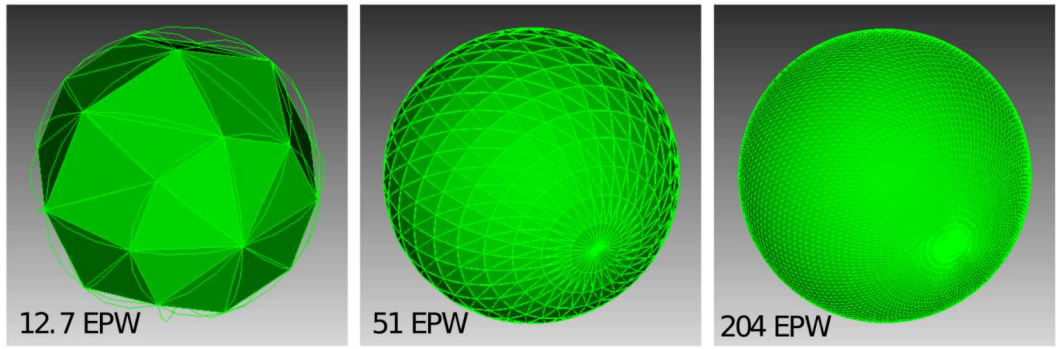

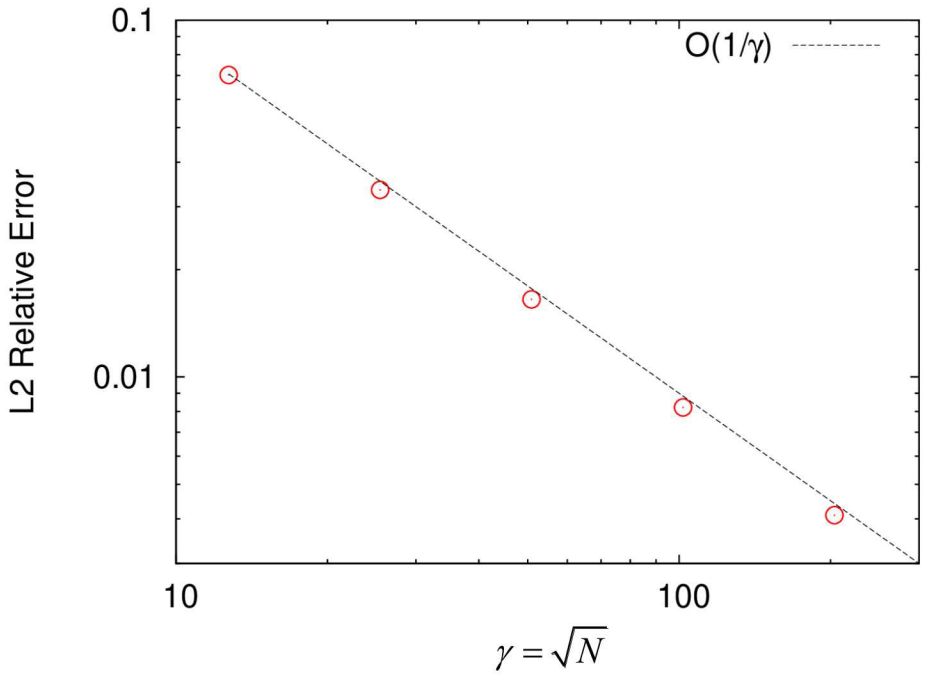

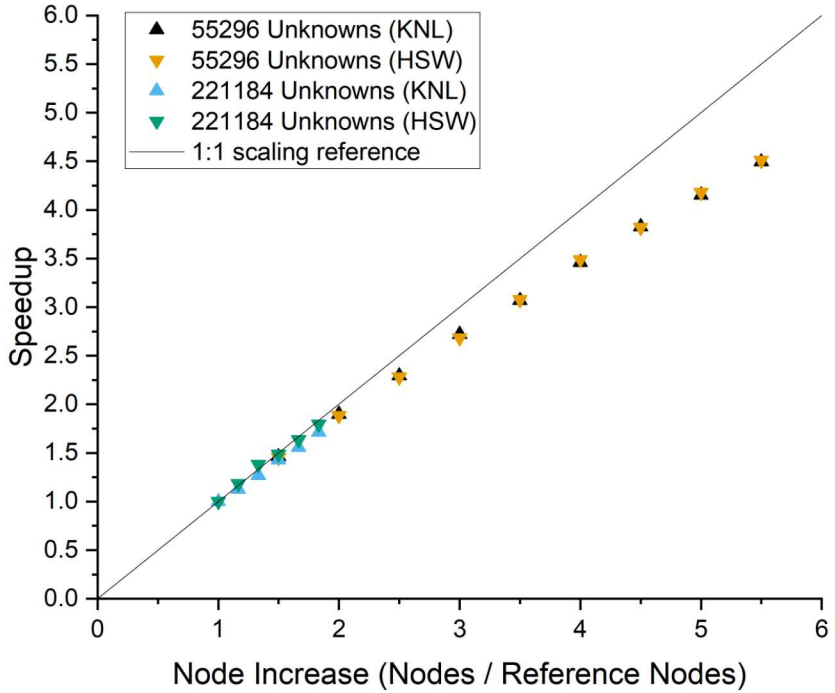

Analytic reference solution for surface current given by Mie scattering solution to Maxwell's equations.

Matrix requires $O(N^2)$ memory to store, calculating its entries is memory bound at the cache level, and $O(N^3)$ computation to solve via LU factorization.

R. Harrington, *Time-Harmonic Electromagnetic Fields*, McGraw-Hill, New York, NY, 1961.

Radar cross section

What is radar cross section?

The radar cross section (RCS) of an object is

$$\sigma = \lim_{R\to\infty} 4\pi R^2 \left|\frac{E^s}{E^i}\right|^2$$

where E^i and E^s are the incident and scattered electric fields, respectively.

Less formally, the RCS is $\sigma = \pi a^2$ where a is the radius of the sphere with the same RCS.

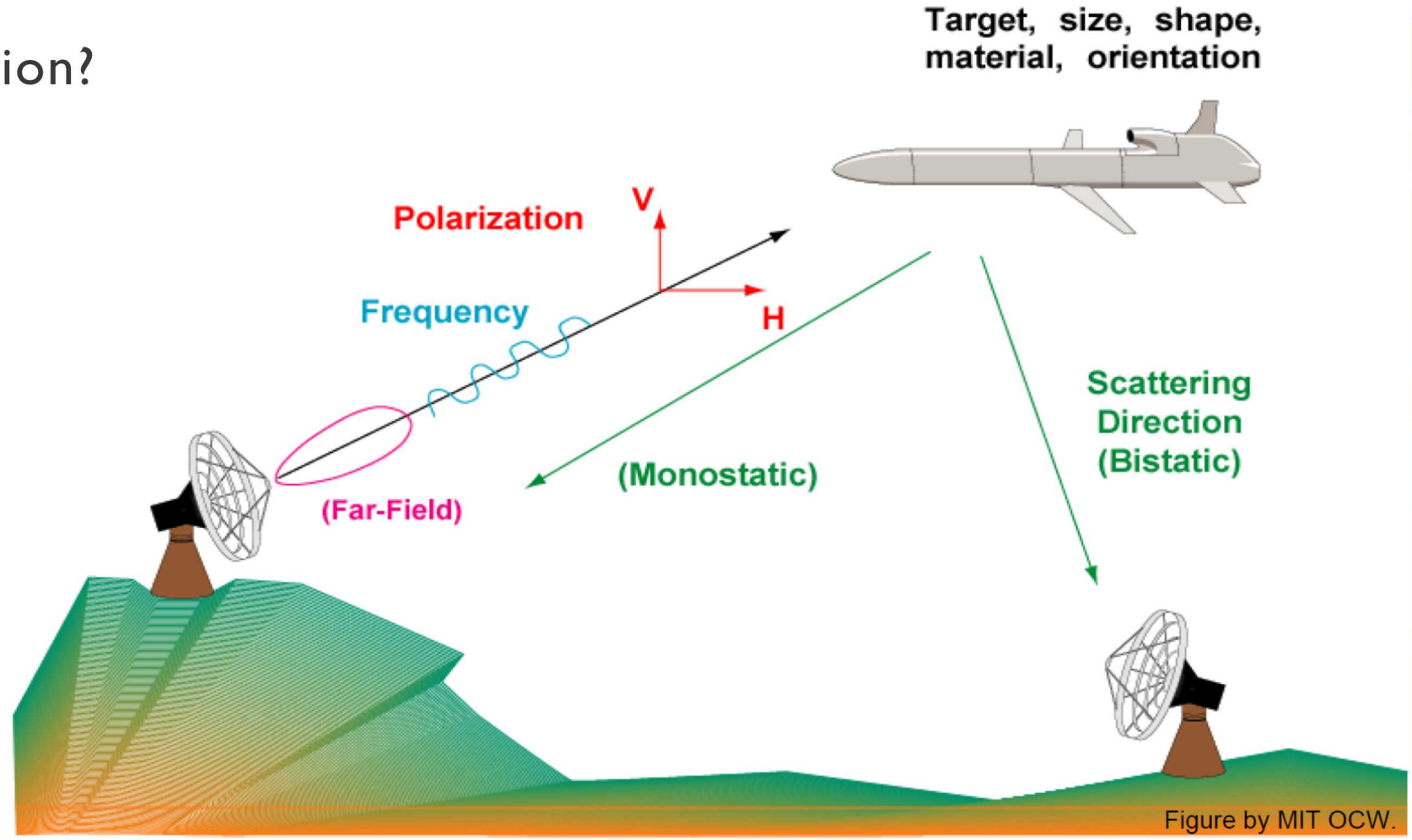

Figure by MIT OCW.

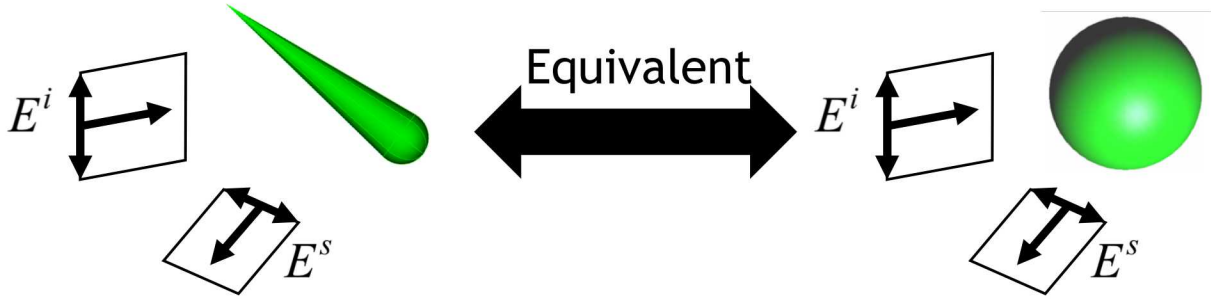

A. E. Fuhs, *Radar Cross Section Lectures*, Naval Postgraduate School, Monterey, CA, 1983, https://apps.dtic.mil/dtic/tr/fulltext/u2/a125576.pdf.

Monostatic RCS for the cone-sphere EMCC object

Electromagnetic Code Consortium (EMCC) data are a standard way to compare. However,

- The data lack information on the experiment setup to reproduce all results nicely, i.e., one can get agreement with the cone-sphere's 9 GHz data, but not the 869 MHz data (below).

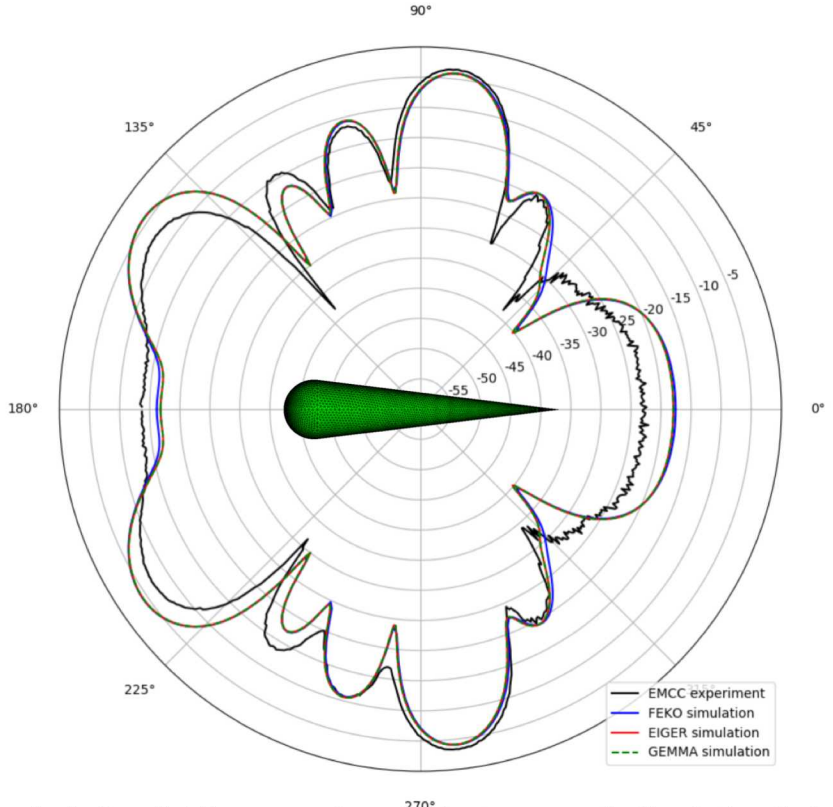

- The data lack error bars associated with taking data from experiment so that the data can be compared with error bars due to running a simulation.
- We need our own experiment data for our use case of interest

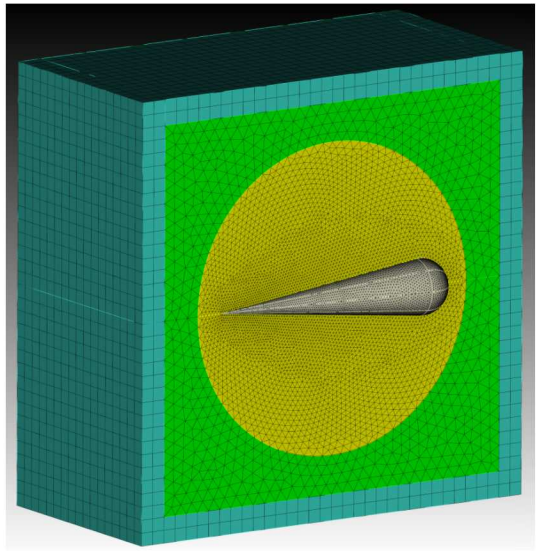

Aside: Performing this simulation with a finite element method (FEM) program required many more elements, but provides many frequencies via a Fourier transform and has a sparse matrix; whether superior to MoM is case dependent.

Langston et al., *Massively Parallel Frequency Domain Electromagnetic Simulation Codes*, Appl. Comput. Electrom. Symposium, 2018.
A. C. Woo, H. T. G. Wang, M. J. Schuh, and M. L. Sanders, "Benchmark Radar Targets for the Validation of Computational Electromagnetics Programs," *IEEE Antennas Propag.*, 35 (1993), pp. 84-89.

Near field

PEC sphere scattering

For the EFIE, the near field is computed without the test integral:

$$E^{total} = E^{inc} + E^{scattered}$$

where

$$E^{scattered}(\boldsymbol{r}) = \sum_n \int_{f_n} \left[i\omega\mu_l \boldsymbol{f}_n(\boldsymbol{r}') - \frac{i}{\omega\epsilon_l} \nabla' \cdot \boldsymbol{f}_n(\boldsymbol{r}') \right] \frac{e^{-ik|\boldsymbol{r}-\boldsymbol{r}'|}}{4\pi|\boldsymbol{r}-\boldsymbol{r}'|}$$

For a 1 m PEC sphere illuminated by a 377 V/m excitation at 4.77 MHz from above, the scattered near field is given on the right.

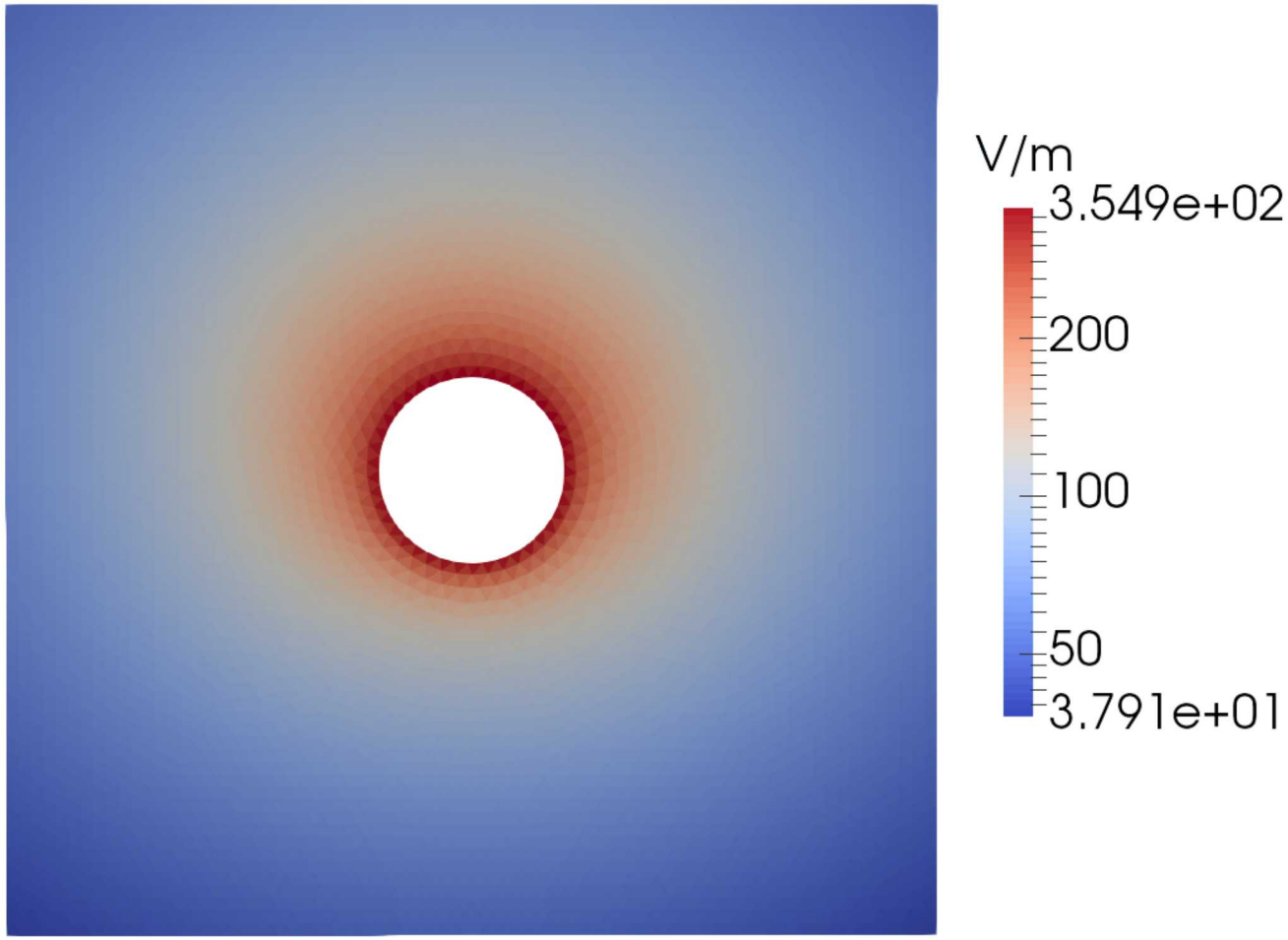

High accuracy integration via a radial angular transformation

The EFIE's $\mathcal{L}$ operator has a weak $O(1/r)$ singularity while the MFIE's $\mathcal{K}$ operator has a strong $O(1/r^2)$ singularity.

$$\mathcal{L}\boldsymbol{X} = [1 + \frac{1}{k^2}\nabla\nabla\cdot]\int G(\boldsymbol{r},\boldsymbol{r}')\boldsymbol{X}(\boldsymbol{r}')d\boldsymbol{r}'$$

$$\mathcal{K}\boldsymbol{X} = \nabla\times\int G(\boldsymbol{r},\boldsymbol{r}')\boldsymbol{X}(\boldsymbol{r}')d\boldsymbol{r}'$$

$$G(r) = \frac{e^{-ikr}}{4\pi r}, \mathrm{r} = |\boldsymbol{r} - \boldsymbol{r}'|$$

For $\mathcal{L}$, we use a radial angular transformation where the source triangle variables of integration become similar to polar coordinates (ρ, ϕ):

$$\int G(\boldsymbol{r},\boldsymbol{r}')\boldsymbol{X}(\boldsymbol{r}')d\boldsymbol{r}' = \int \frac{e^{-ikr}}{4\pi r}\boldsymbol{X}(r,u)\frac{r}{\cosh u}drdu\,,$$

$$u = \ln\tan^{-1}(\phi/2)$$

For $\mathcal{K}$, in addition to a radial angular transformation, we subtract the first term of the integrand's Taylor series. This is similar to

$$\int \frac{e^r}{r}dr = \int \frac{e^r - 1}{r}dr - \int \frac{1}{r}dr \text{ where}$$

$$\frac{e^r - 1}{r} = \frac{(1 + r + r^2 + \cdots) - 1}{r} = \frac{r + r^2 + \cdots}{r}$$

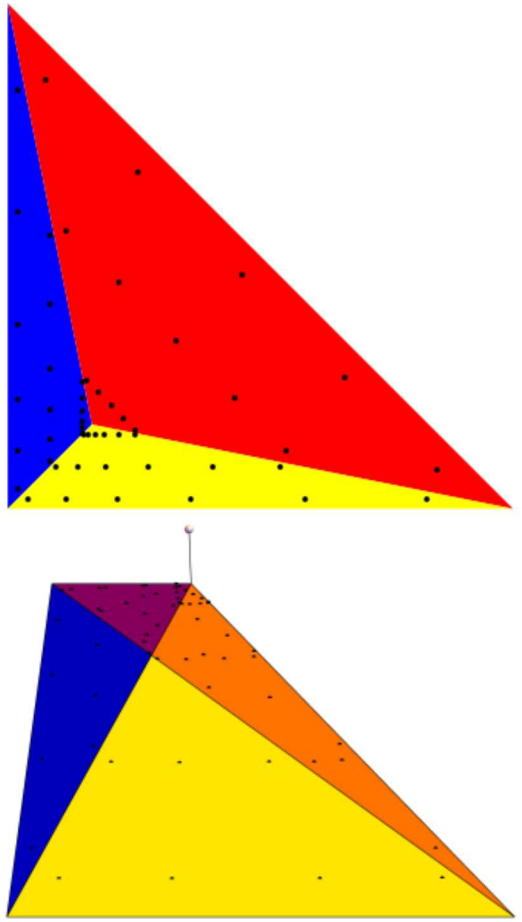

The 3 subtriangles used in the radial angular transformation when the singularity is interior and exterior to the triangle.

M. A. Khayat and R. D. Wilton, "An Improved Tansformation and Optimized Sampling Scheme for the Numerical Evaluation of Singular and Near-Singular Potentials," *IEEE Antennas Wirel. Propag. Lett.*, 7 (2008), pp. 377 - 380.

Near field for airplane intakes

Top right: Direct solve by LU factorization.
Bottom right: Solve by adaptive cross approximation (ACA).

While intake fields are much higher than incident fields, fast methods can often obtain qualitatively good results for this near field calculation.

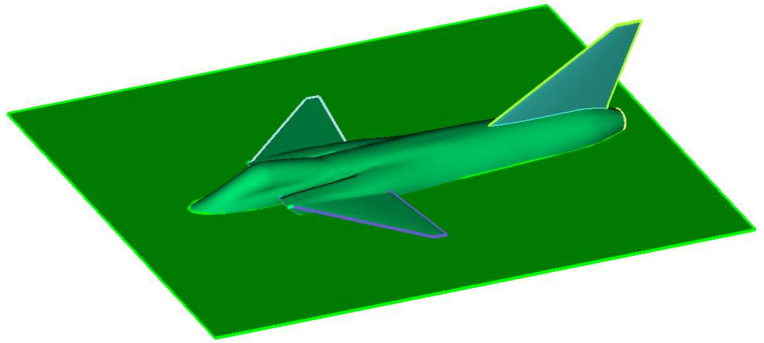

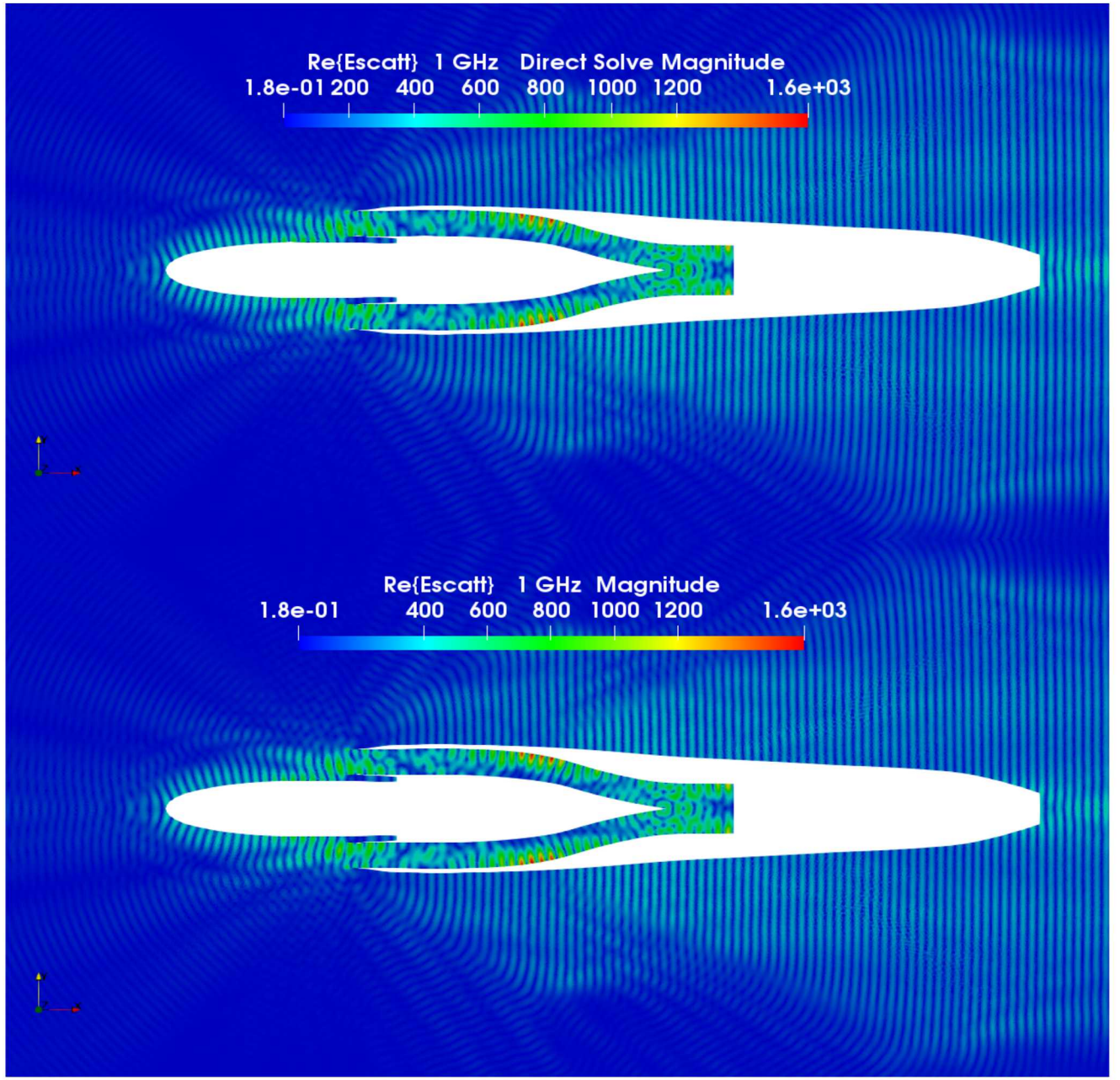

Cavity problem

Thin PEC hollow sphere at a higher frequency than the PEC sphere

Top:
- Solid sphere
- 4.77 MHz excitation from above, magnitude 1 V/m

Bottom left:
- Hollow sphere
- 130 MHz excitation from above, magnitude 1 V/m

Bottom right:
- Hollow sphere
- 130 MHz excitation from below, magnitude 1 V/m

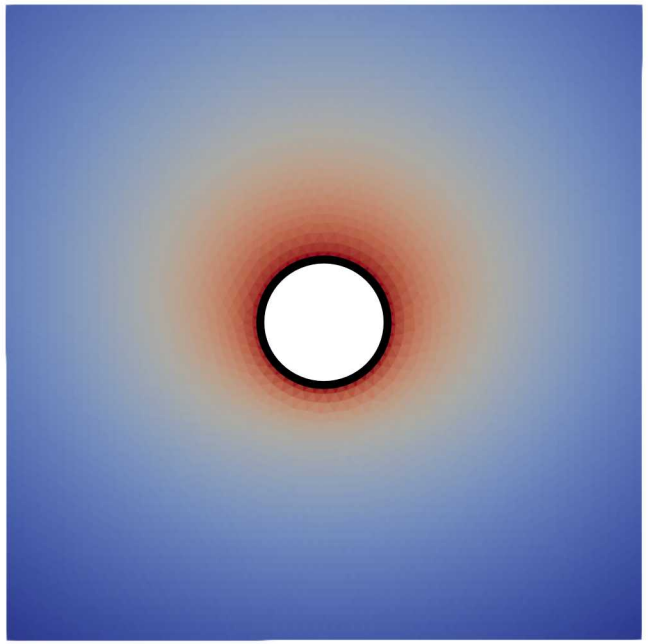

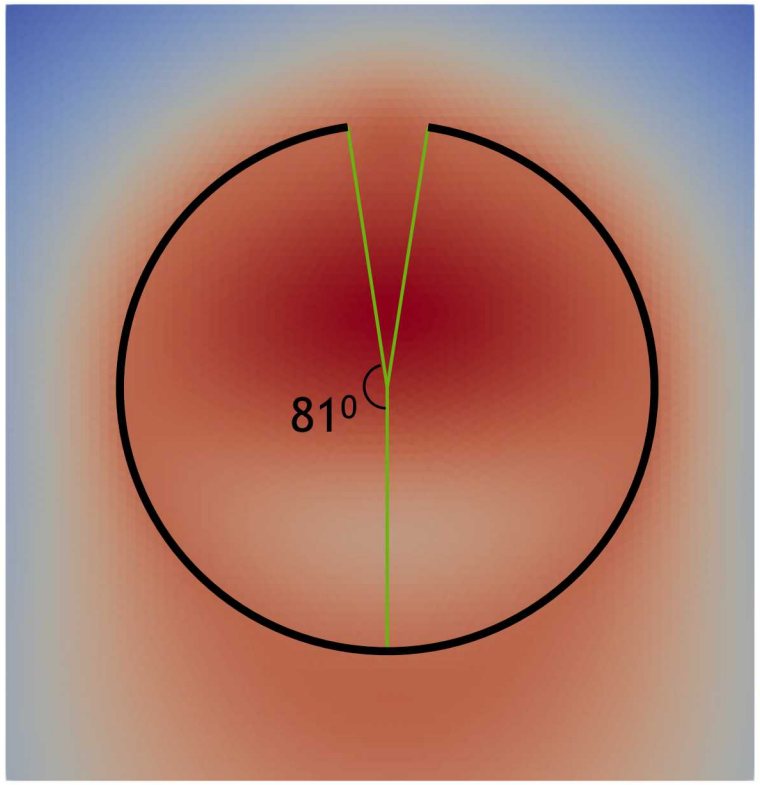

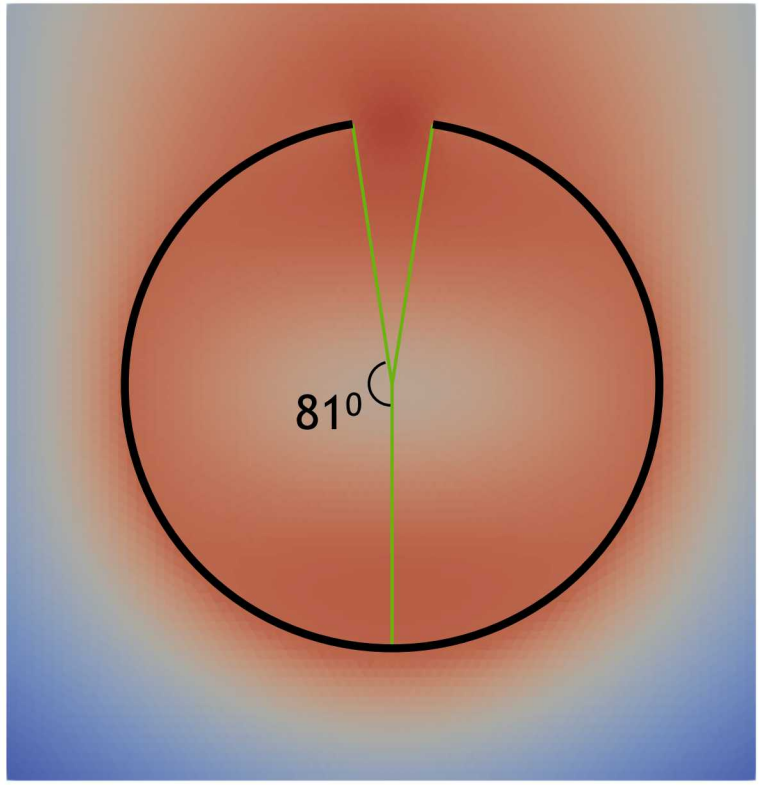

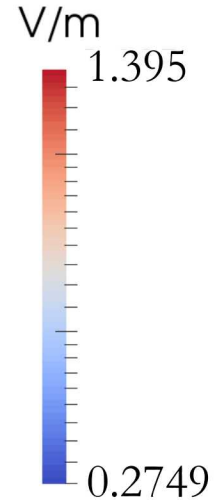

Electromagnetic radiation (EMR) coupling to high Q cavities

$$Q = \omega \frac{\text{energy stored}}{\text{average power dissipated}}$$

Shielding effectiveness is defined by
SE = 20 $\log_{10}$ (interior field / exterior field)

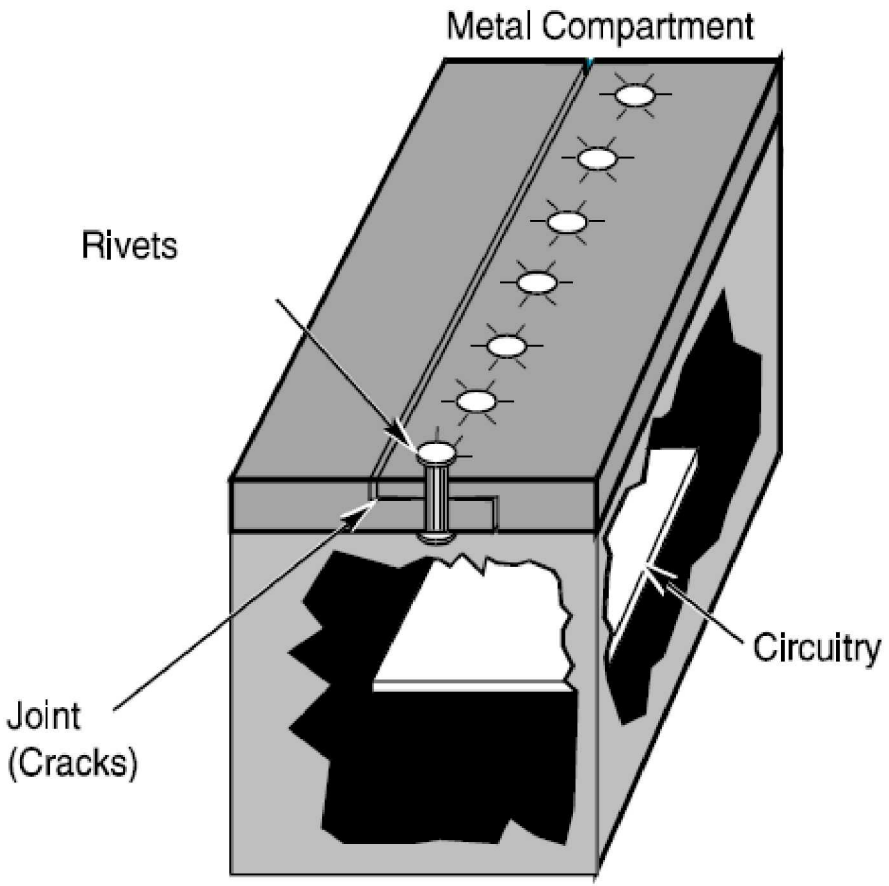

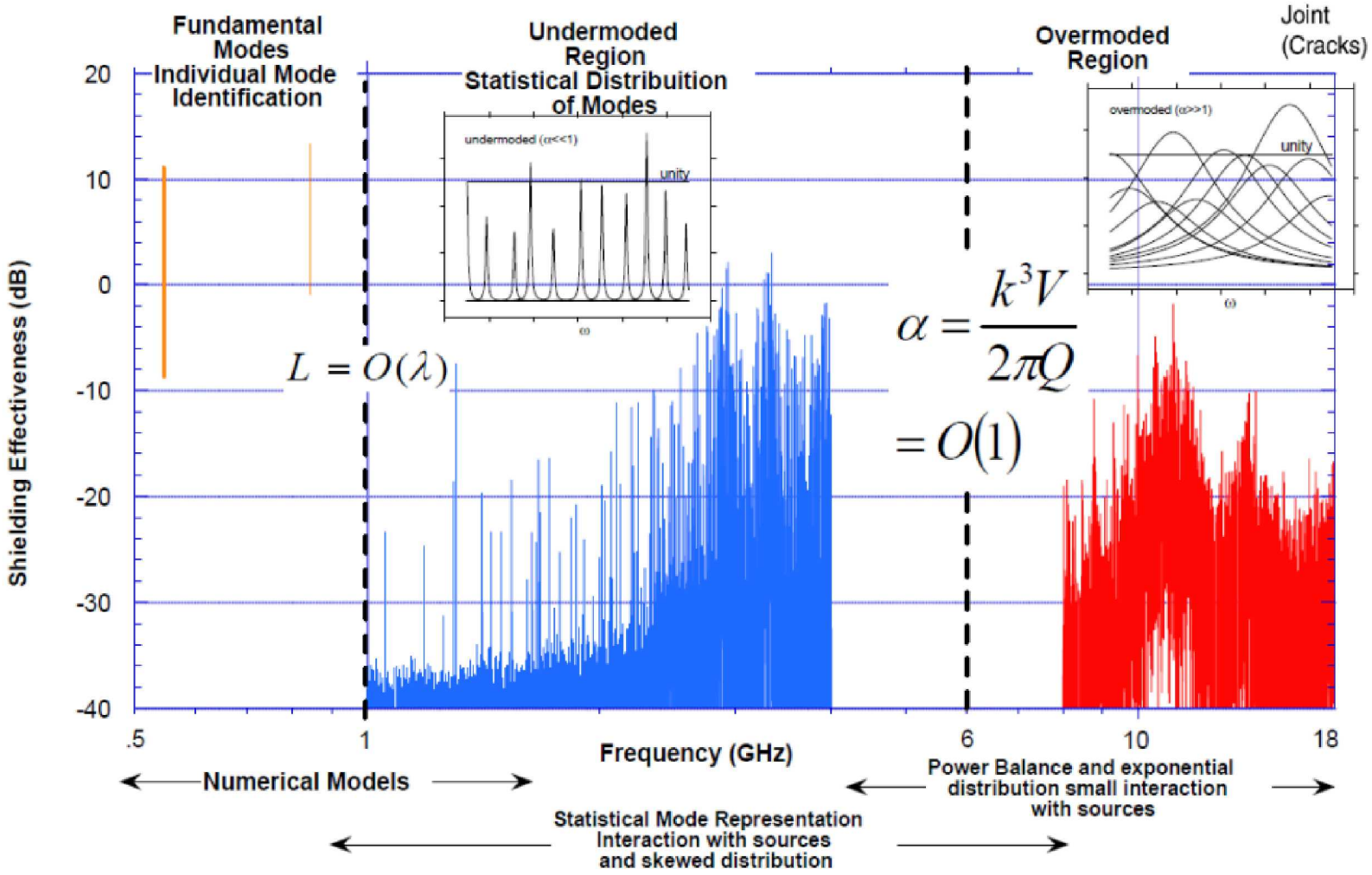

S. Campione et al., *Preliminary Survey on the Effectiveness of an Electromagnetic Dampener to Improve System Shielding Effectiveness*, Sandia Technical Report SAND2018-10548, 2018.

Slot subcell model for capturing coupling into a cavity accurately

In free space, the thin slot equation is:

$$H_z^{>}(a,z)+\frac{1}{4}\left(\Delta Y_C \frac{d^2}{dz^2} I_m - \Delta Y_L I_m\right) = -H_z^{inc}(z), I_m = -2V$$

H_z = magnetic field

I_m = current

V = voltage

a = equivalent radius

Y_C, Y_L capture gaskets and wall loss

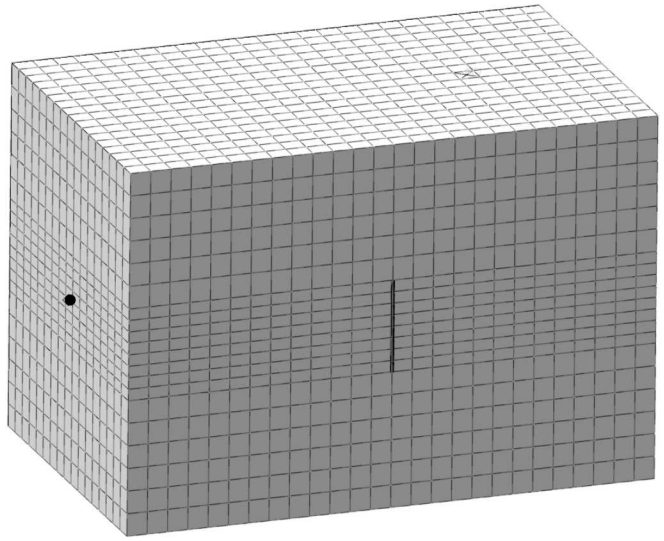

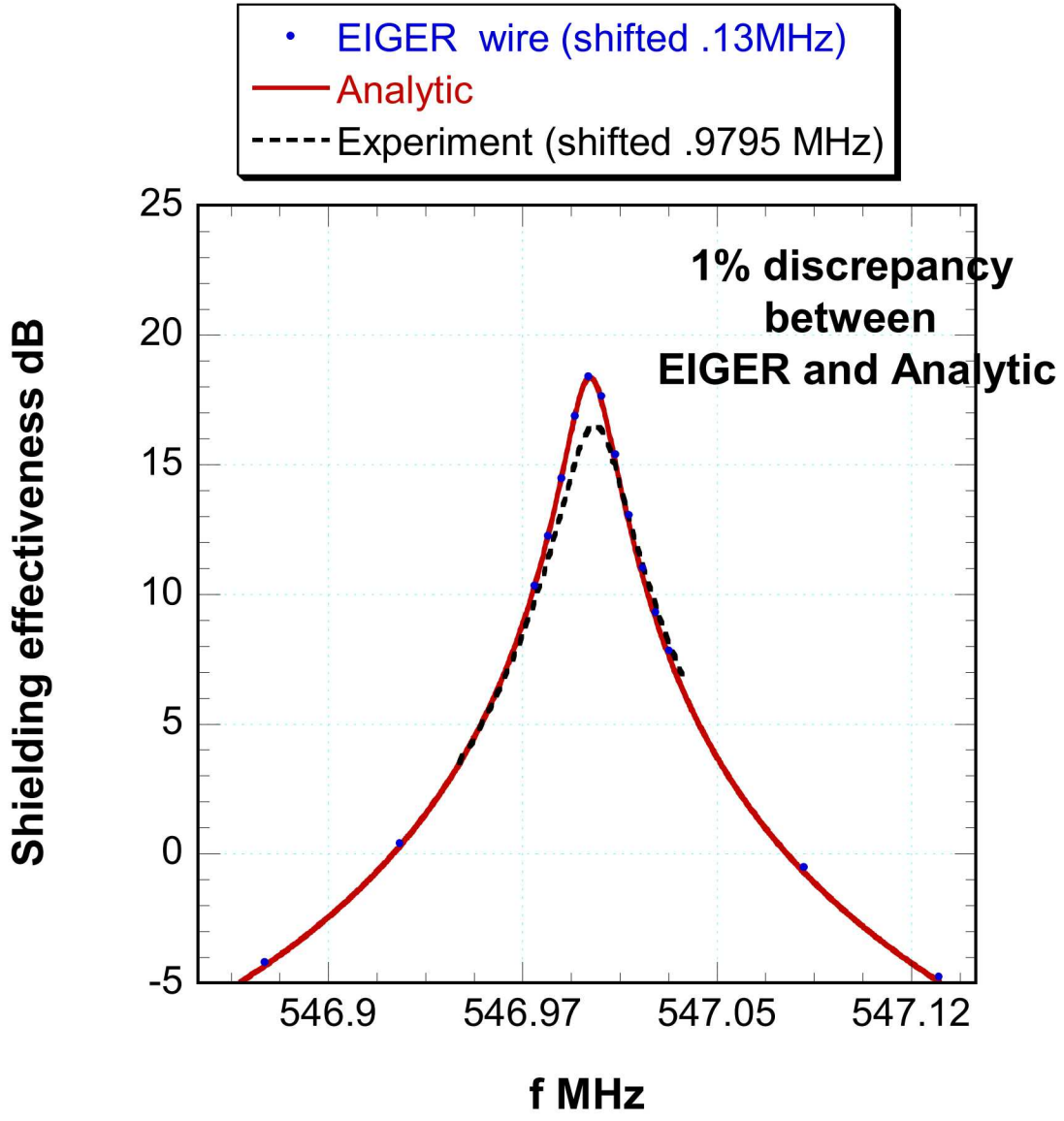

Cavity comparison with analytic and experiment

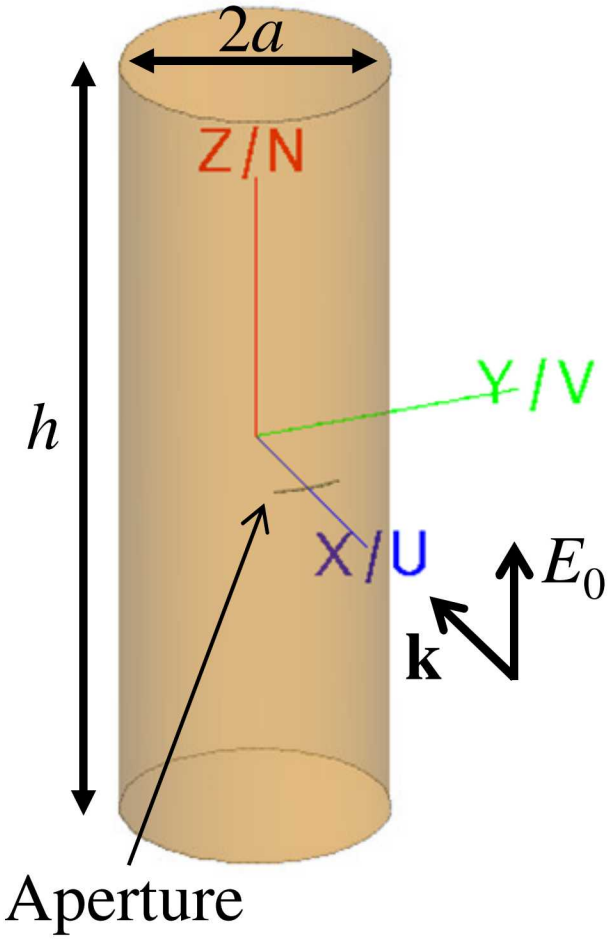

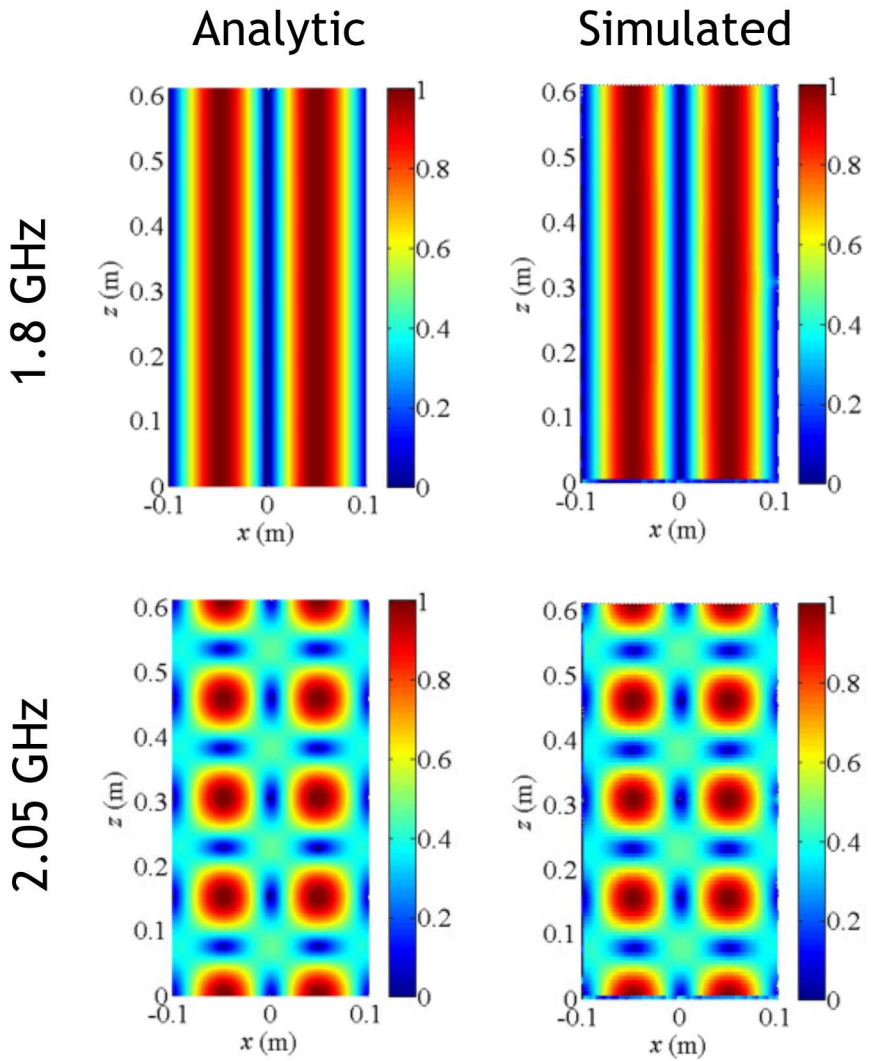

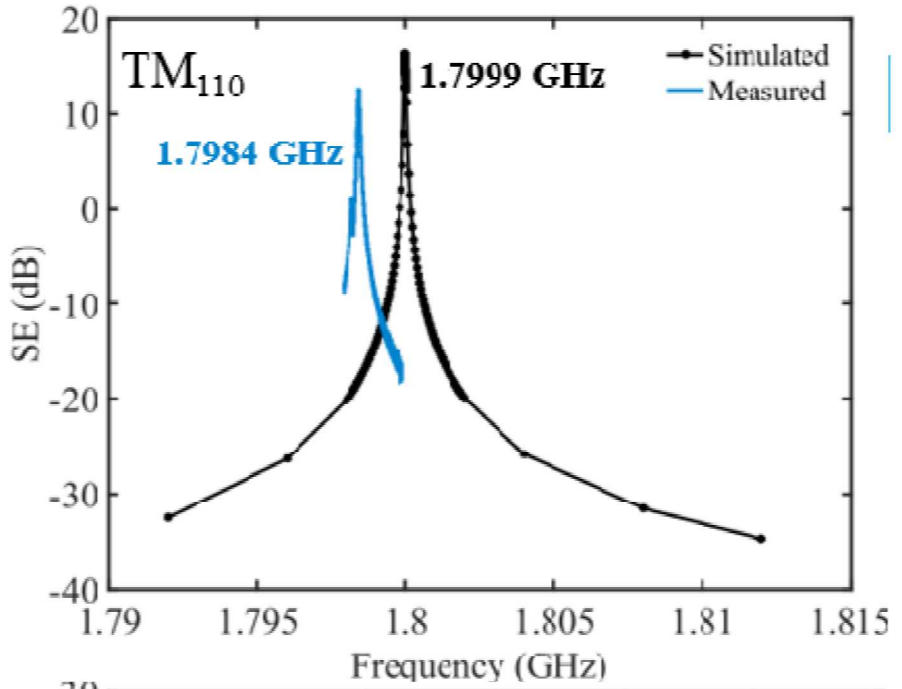

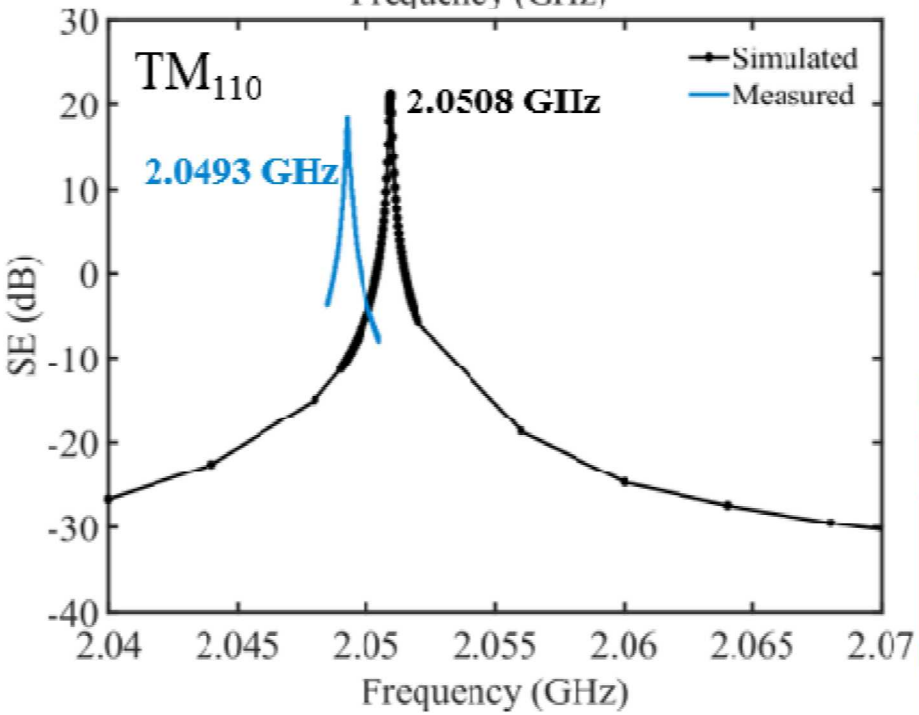

S. Campione et al., *Preliminary Survey on the Effectiveness of an Electromagnetic Dampener to Improve System Shielding Effectiveness*, Sandia Technical Report SAND2018-10548, 2018.

Response for centered slot vs slightly off-center slot

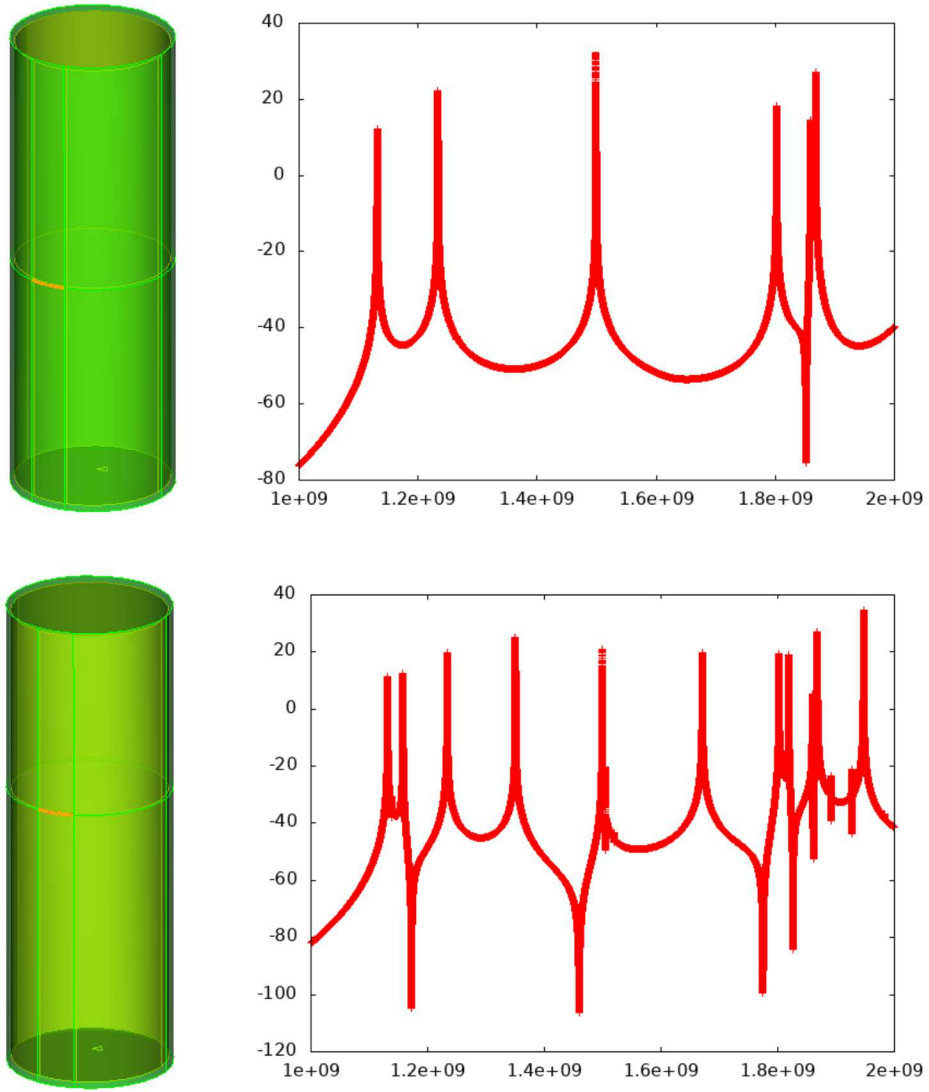

Power balance can be used to obtain an unmatched bound on the SE by equating the power received with the power lost due to the interior cavity wall, interior antennas, energy escaping out the slot, and other causes:

$$P_{rec} = P_{wall} + P_{ant} + P_{out} + \ldots$$

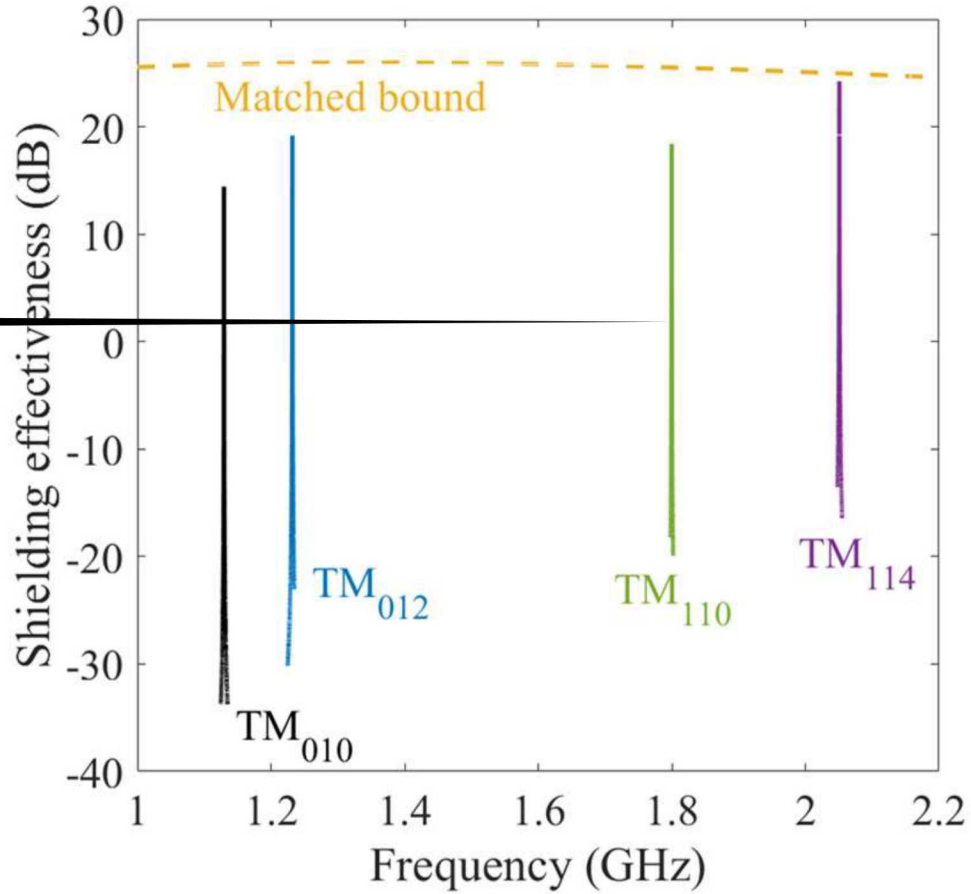

S. Campione et al., *Penetration through Slots in Cylindrical Cavities Operating at Fundamental Cavity Modes*, in review.

Dealing with uncertainties

Dakota is a Sandia code that facilitates the exploration of parameter spaces for uncertainty quantification, optimization, and other purposes.

Right: Slot parameter sweeps using EIGER and the unmatched formulation.

Below: Future automated runs using Gemma with parameter sweeps.

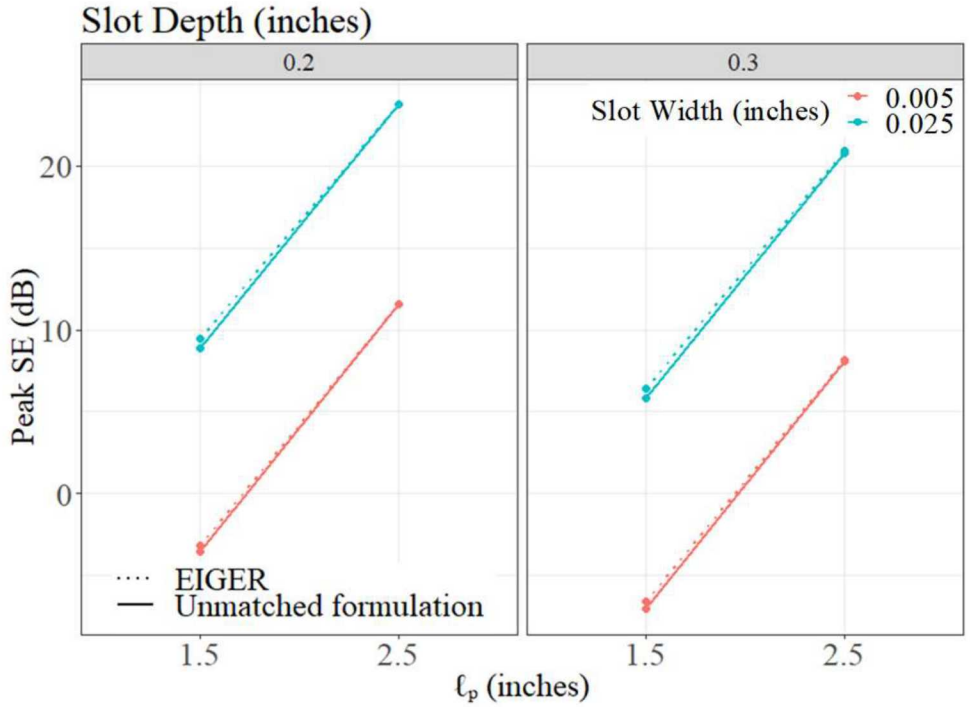

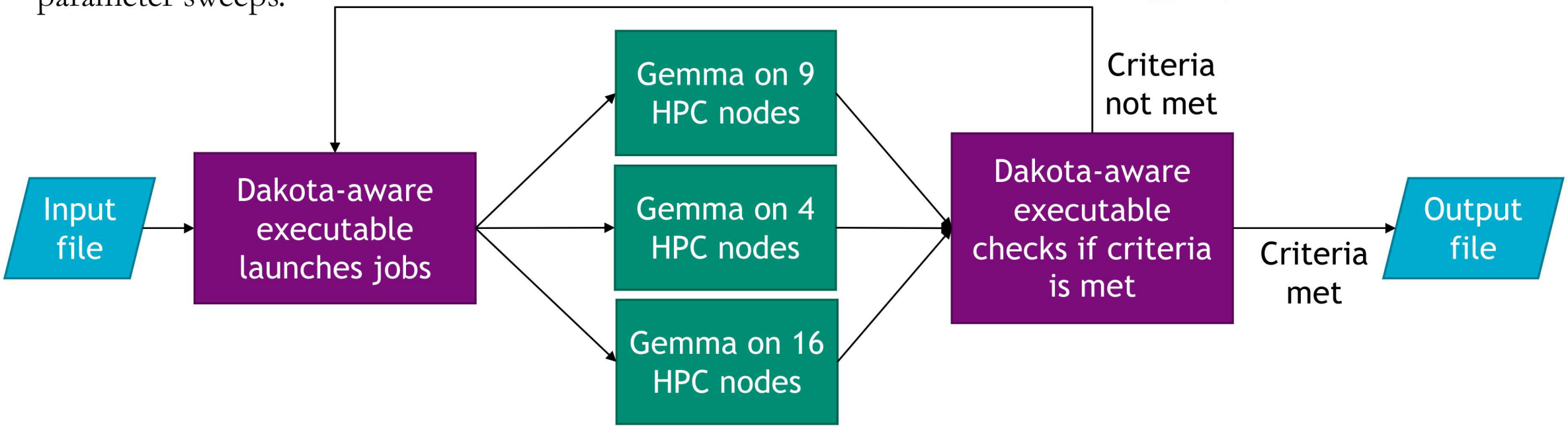

B. M. Adams, "Dakota, A Multilevel Parallel Object-Oriented Framework for Design Optimization, Parameter Estimation, Uncertainty Quantification, and Sensitivity Analysis: Version 6.0 Theory Manual," Sandia Technical Report SAND2014-4253, 2014.
S. Campione et al., *Penetration through Slots in Cylindrical Cavities Operating at Fundamental Cavity Modes*, in review.

Weak scalability for Adelus, **A** Dense **LU** Solver Package

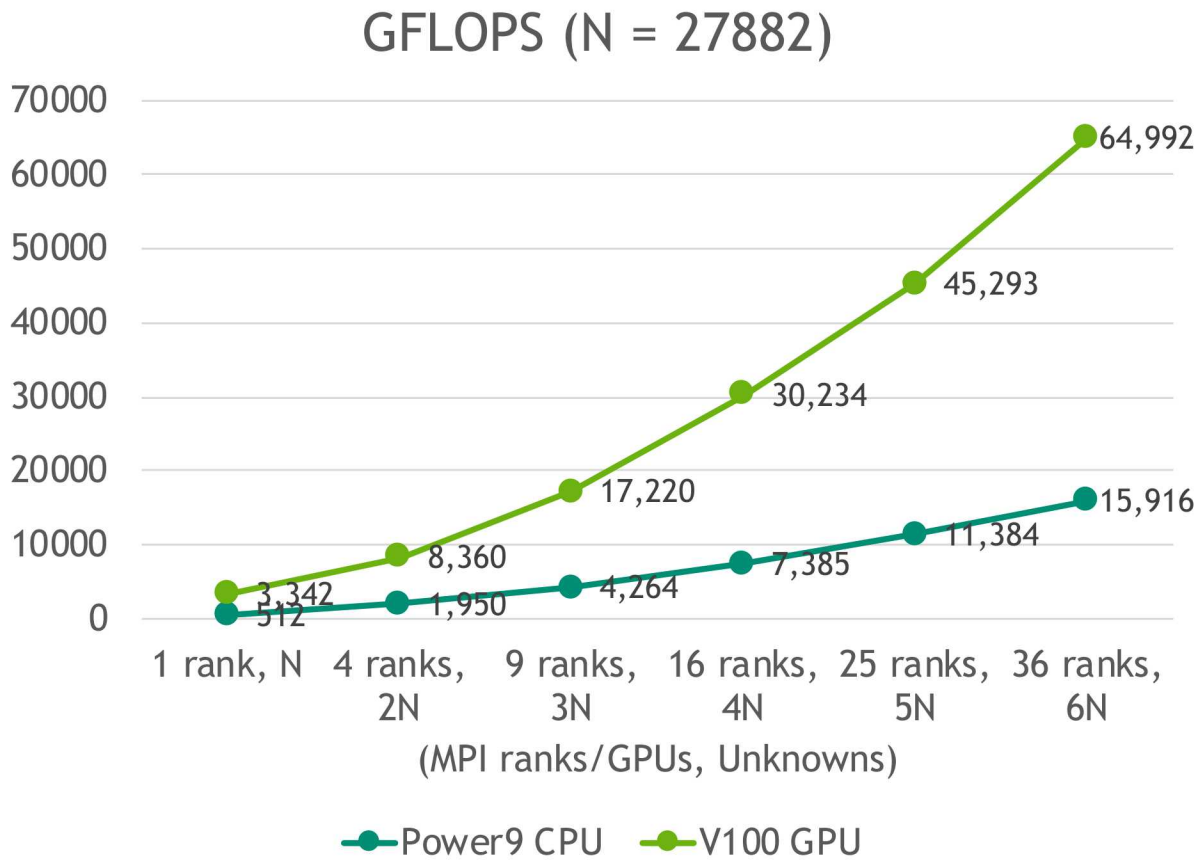

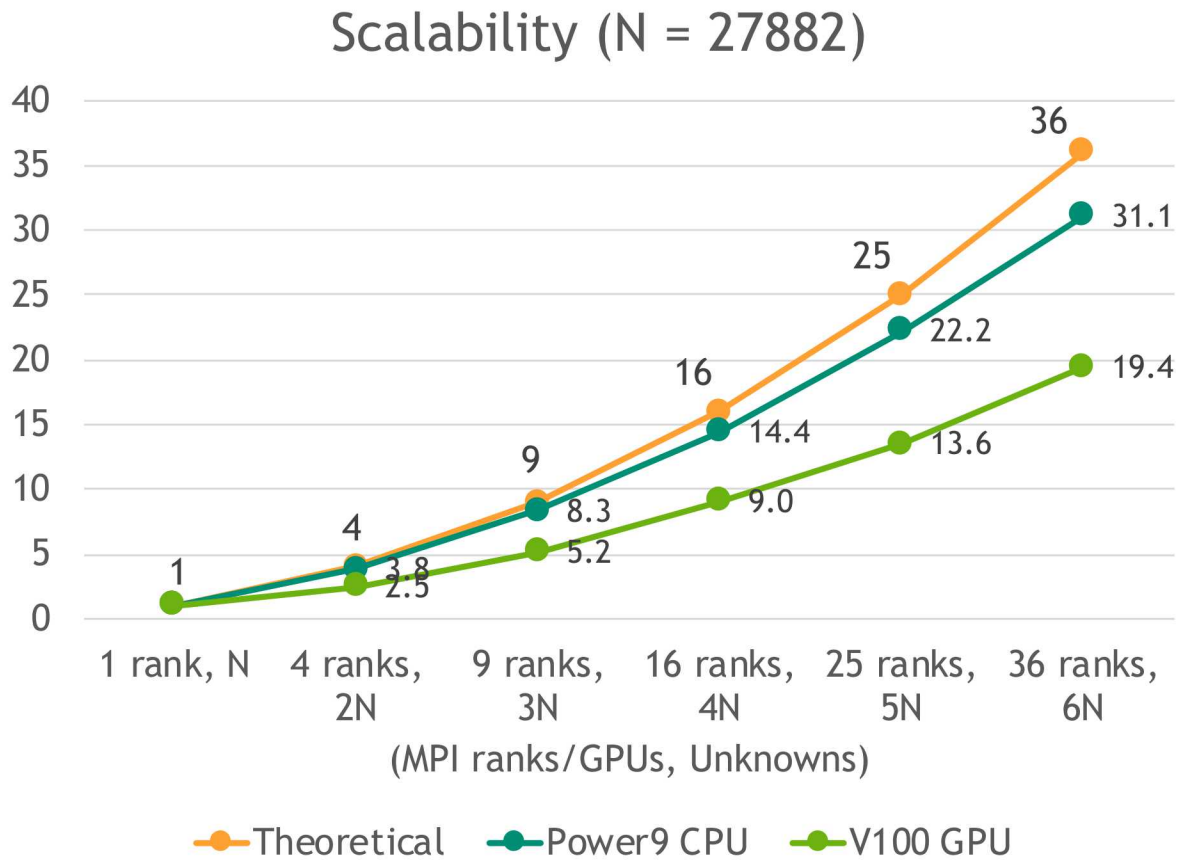

$$S = \frac{\text{GFLOPS(ranks/GPUs,unknowns)}}{\text{GFLOPS(1,1N)}}$$

where ranks/GPUs = 1, 4, 9, 16, 25, 36
and unknowns = 1N, 2N, 3N, 4N, 5N, 6N

How to guarantee these capabilities after each source code change?

Nightly, weekly, or even monthly testing of problems on local and HPC resources for each use case.

VVtest is a Sandia-developed set of scripts that automate the testing of complex simulation runs, like those required for verification, validation, and uncertainty quantification.

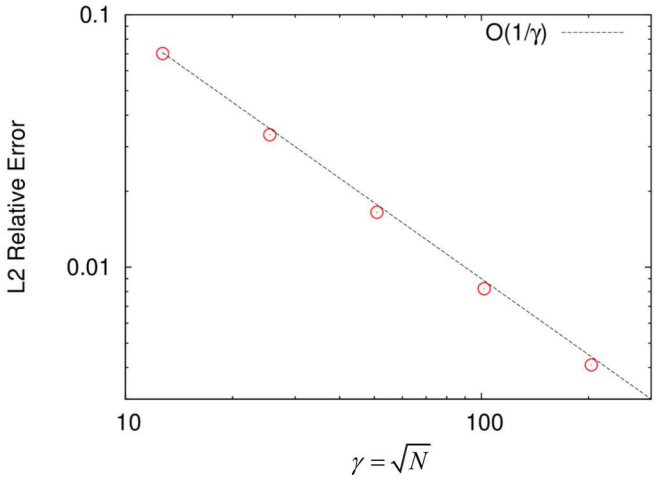

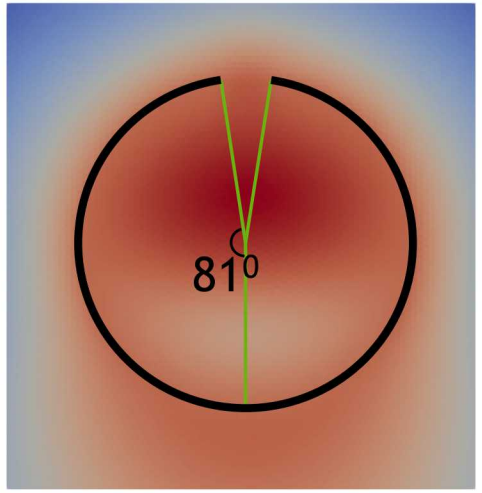

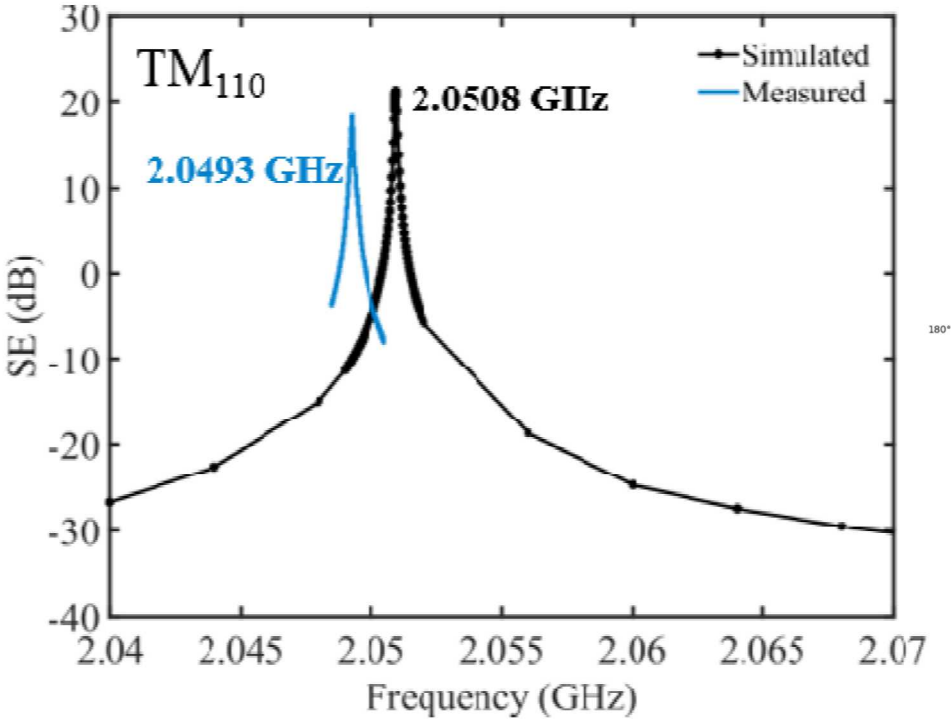

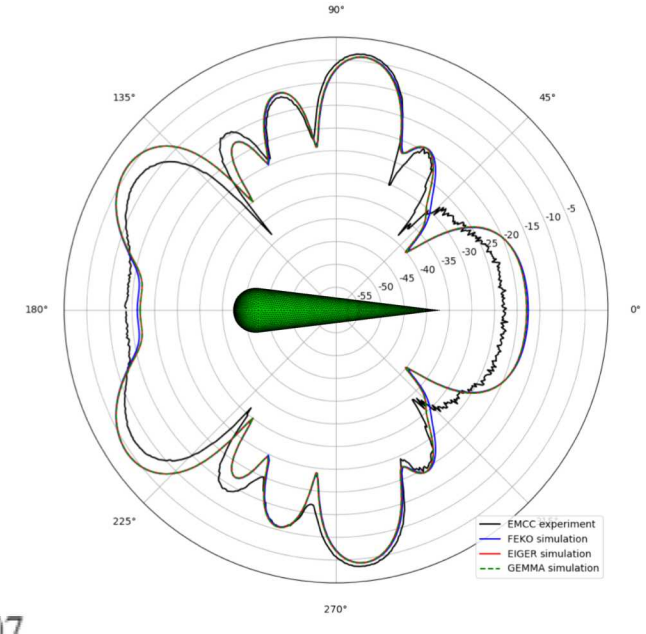

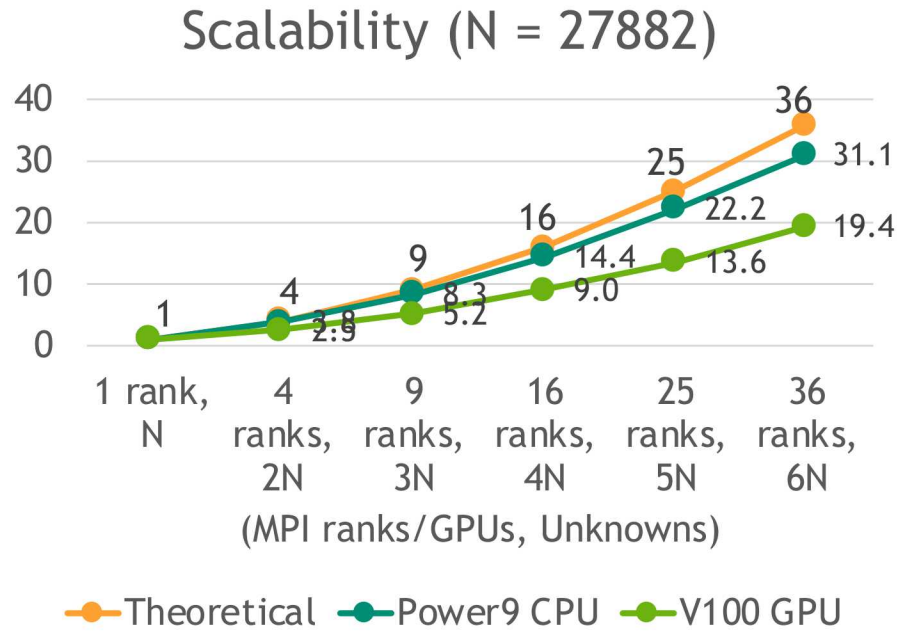

Thank you!

Bibliography

R. Harrington, *Time-Harmonic Electromagnetic Fields*, McGraw-Hill, New York, NY, 1961.

H. C. Edwards, C. R. Trott, and D. Sunderland, "Kokkos: Enabling manycore performance portability through polymorphic memory access patterns," *Journal of Parallel and Distributed Computing*, 74 (2014), pp. 3202-3216.

A. E. Fuhs, *Radar Cross Section Lectures,* Naval Postgraduate School, Monterey, CA, 1983, https://apps.dtic.mil/dtic/tr/fulltext/u2/a125576.pdf.

MIT OCW

A. C. Woo, H. T. G. Wang, M. J. Schuh, and M. L. Sanders, "Benchmark Radar Targets for the Validation of Computational Electromagnetics Programs," *IEEE Antennas Propag.,* 35 (1993), pp. 84-89.

M. A. Khayat and R. D. Wilton, "An Improved Tansformation and Optimized Sampling Scheme for the Numerical Evaluation of Singular and Near-Singular Potentials," *IEEE Antennas Wirel. Propag. Lett.*, 7 (2008), pp. 377 - 380.

S. Campione et al., *Preliminary Survey on the Effectiveness of an Electromagnetic Dampener to Improve System Shielding Effectiveness*, Sandia Technical Report SAND2018-10548, 2018.

S. Campione et al., *Penetration through Slots in Cylindrical Cavities Operating at Fundamental Cavity Modes*, in review.

B. M. Adams, "Dakota, A Multilevel Parallel Object-Oriented Framework for Design Optimization, Parameter Estimation, Uncertainty Quantification, and Sensitivity Analysis: Version 6.0 Theory Manual," Sandia Technical Report SAND2014-4253, 2014.

Additional slides

Depiction of surface current on a boundary between regions

Recall that the EFIE is

$$Z_{m,n} = \int_{f_m}\int_{f_n}\left[i\omega\mu_l \boldsymbol{f}_m \cdot \boldsymbol{f}_n - \frac{i}{\omega\epsilon_l}\nabla\cdot\boldsymbol{f}_m\nabla'\cdot\boldsymbol{f}_n\right]\frac{e^{-ikr}}{4\pi r}$$

with basis functions

$$\mathbf{f_n}(\mathbf{r}) = \begin{cases} \frac{\ell_n}{2A_n^+}\boldsymbol{\rho_n^+} & \mathbf{r}\in T_n^+ \\ \frac{\ell_n}{2A_n^-}\boldsymbol{\rho_n^-} & \mathbf{r}\in T_n^- \\ \mathbf{0} & \text{otherwise} \end{cases}$$

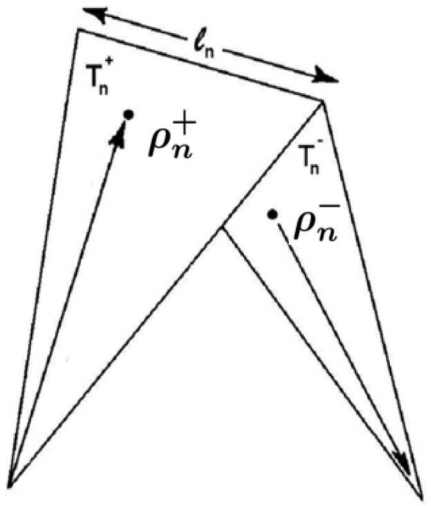

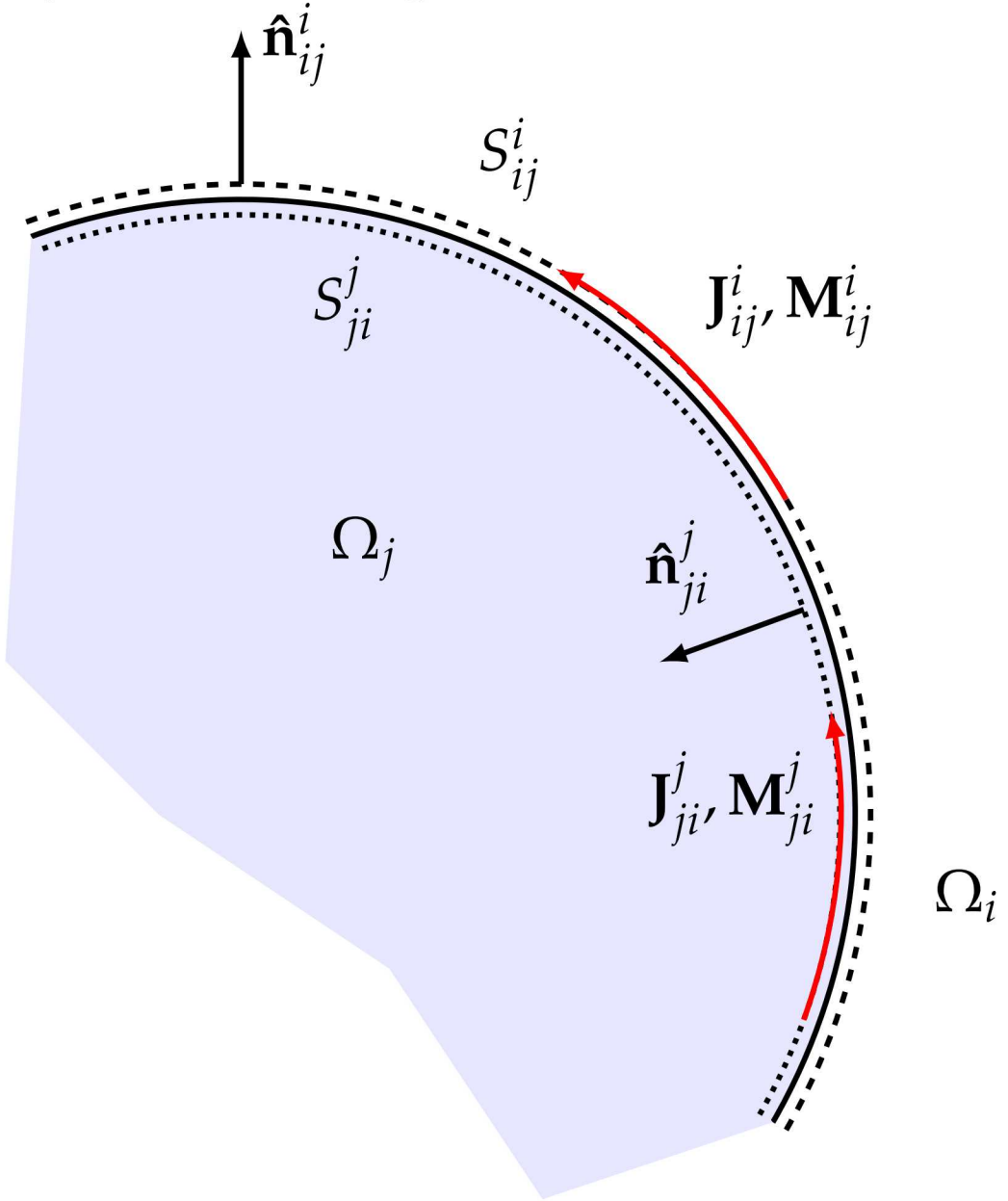

Maxwell's Equations in the Frequency Domain

$\exp(j\omega t)$ time harmonic convention

$$\text{Faraday}: \quad \nabla \times \mathbf{E} = -j\omega\mathbf{B}$$

$$\text{Ampere} - \text{Maxwell}: \quad \nabla \times \mathbf{H} = \mathbf{J} + j\omega\mathbf{D}$$

$$\text{Electric Gauss}: \quad \nabla \cdot \mathbf{D} = \rho$$

$$\text{Magnetic Gauss}: \quad \nabla \cdot \mathbf{B} = 0$$

$\mathbf{E}$: electric field [V/m]
$\mathbf{H}$: magnetic field [A/m]
$\mathbf{D}$: electric flux density [C/m^2]
$\mathbf{B}$: magnetic flux density [T = Wb/m^2]
$\mathbf{J}$: electric current density [A/m^2]
ρ : volume charge density [C/m^3]

Constitutive relations:

$\mathbf{D} = \epsilon\mathbf{E}$ $\quad \epsilon$: permitivity [F/m]
$\mathbf{B} = \mu\mathbf{H}$ $\quad \mu$: permeability [H/m]
$\mathbf{J} = \sigma\mathbf{E}$ $\quad \sigma$: conductivity [S/m]

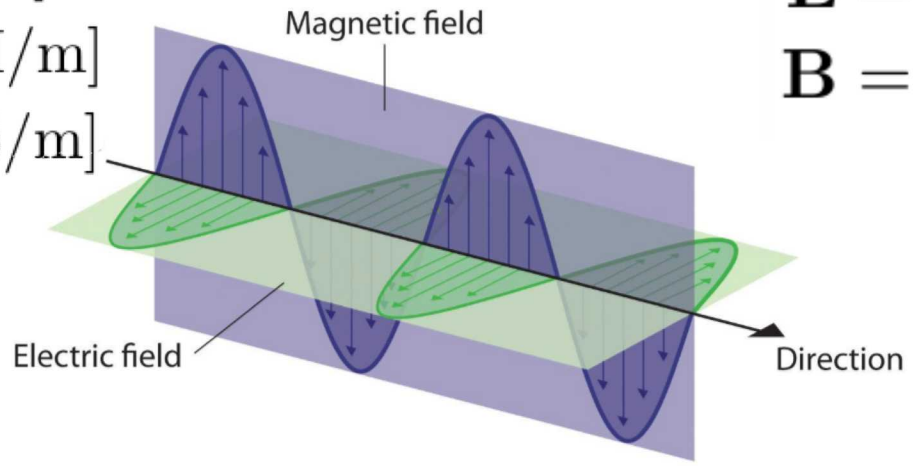

Vector & Scalar Potentials:

$$\mathbf{E} = -j\omega\mathbf{A} - \nabla\Phi$$
$$\mathbf{B} = \nabla \times \mathbf{A}$$

Lorentz Gauge:

$$\nabla \cdot \mathbf{A} = -j\omega\epsilon\mu\Phi$$

Magnetic Vector & Scalar Potentials and Green's Function

Wave Equations:

$$\nabla^2 \mathbf{A} + \omega^2 \mu\epsilon \mathbf{A} = -\mu \mathbf{J}$$

$$\nabla^2 \Phi + \omega^2 \mu\epsilon \Phi = \rho/\epsilon$$

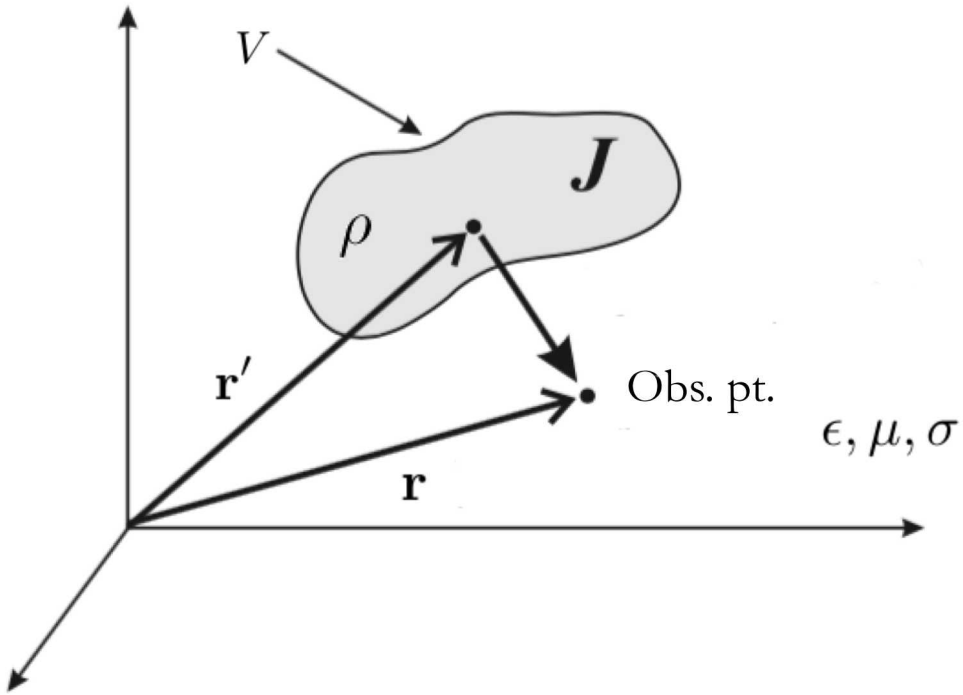

For a linear homogeneous, unbounded medium:

$$\mathbf{A} = \int_V \mu \mathbf{J}(\mathbf{r}') g(\mathbf{r}|\mathbf{r}') dv'$$

$$\Phi = -\int_V \frac{\rho(\mathbf{r}')}{\epsilon} g(\mathbf{r}|\mathbf{r}') dv'$$

Free-Space Green's Function:

$$g(\mathbf{r}|\mathbf{r}') = \frac{e^{-jk|\mathbf{r}-\mathbf{r}'|}}{4\pi|\mathbf{r}-\mathbf{r}'|}$$

Radiation condition enforced

Integral Equations (Boundary Element Method – BEM)

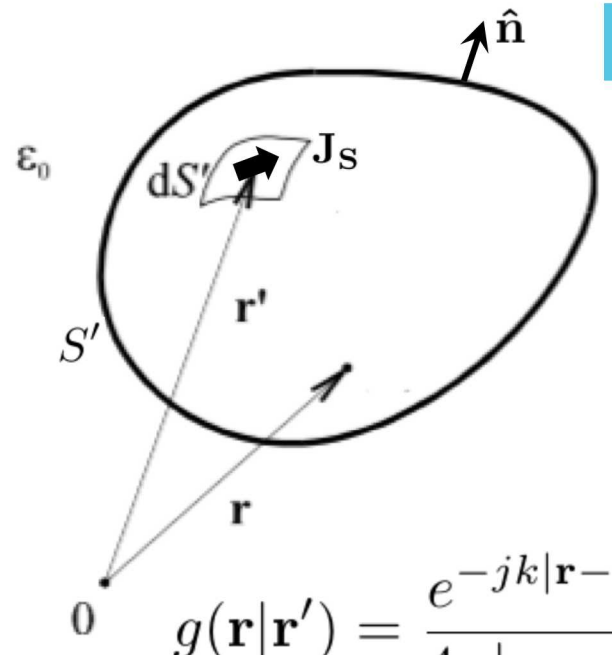

Example of an electric field integral equation (EFIE) for metallic scatterer:

Enforcing the boundary condition at the surface:

$$\hat{\mathbf{n}} \times (\mathbf{E_{inc}} + \mathbf{E_{scat}}) = \mathbf{0}$$

where,

$$\mathbf{E_{scat}} = -j\omega\mu \int_{S'} \left(\mathbf{J_S}(\mathbf{r}')g(\mathbf{r}|\mathbf{r}') + \frac{1}{\omega^2\mu\epsilon}\nabla' \cdot \mathbf{J_S}(\mathbf{r}')\nabla g(\mathbf{r}|\mathbf{r}') \right) ds'$$

$$g(\mathbf{r}|\mathbf{r}') = \frac{e^{-jk|\mathbf{r}-\mathbf{r}'|}}{4\pi|\mathbf{r}-\mathbf{r}'|}$$

results in the following integral equation:

$$\int_{S'} \hat{\mathbf{n}} \times \left(\mathbf{J_S}(\mathbf{r}')g(\mathbf{r}|\mathbf{r}') + \frac{1}{\omega^2\mu\epsilon}\nabla' \cdot \mathbf{J_S}(\mathbf{r}')\nabla g(\mathbf{r}|\mathbf{r}') \right) ds' = \frac{1}{j\omega\mu}\hat{\mathbf{n}} \times \mathbf{E_{inc}}$$

$$L\{\mathbf{J_S}\} = \frac{1}{j\omega\mu}\hat{\mathbf{n}} \times \mathbf{E_{inc}}$$

Method of Moments (MoM)

Numerical solution of integral equation:

$$L\{\mathbf{J_S}\} = \frac{1}{j\omega\mu}\hat{\mathbf{n}} \times \mathbf{E_{inc}}$$

Discretize the scatterer

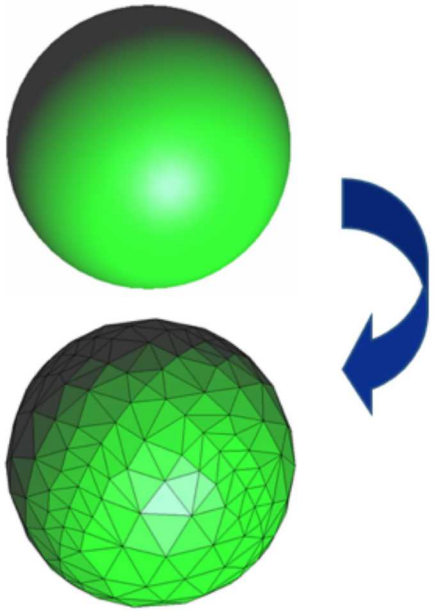

Expand unknown in a set of basis functions.

$$\mathbf{J_S}(\mathbf{r}) \approx \sum_n I_n \mathbf{f_n}(\mathbf{r})$$

$$\mathbf{f_n}(\mathbf{r}) = \begin{cases} \frac{\ell_n}{2A_n^+}\boldsymbol{\rho}_n^+ & \mathbf{r} \in T_n^+ \\ \frac{\ell_n}{2A_n^-}\boldsymbol{\rho}_n^- & \mathbf{r} \in T_n^- \\ \mathbf{0} & \text{otherwise} \end{cases}$$

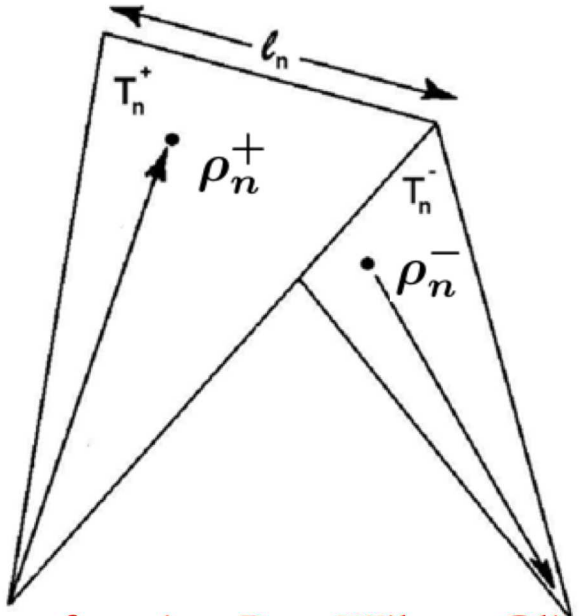

Divergence-conforming Rao-Wilton-Glisson (RWG) basis functions

Test integral equation with basis functions.

$$\int_S \mathbf{f_m} \cdot L\{\mathbf{J_S}\}\, ds = \frac{1}{j\omega\mu}\int_S \mathbf{f_m} \cdot (\hat{\mathbf{n}} \times \mathbf{E_{inc}})\, ds$$

$$\overline{\mathbf{Z}}\mathbf{I} = \mathbf{V}$$

EIGER Formulation

Test with basis functions (Galerkin method)

Integral equation becomes a matrix equation:

$$Z_{N\times N} I_{N\times M} = V_{N\times M}$$

N is the total number of current unknowns

M is the number of independent excitations

Note that the matrix Z is, in general, **dense** and **complex valued**.

- N^2 double complex matrix entries

Monostatic RCS results (1.57 GHz)

"hh"

"vv"

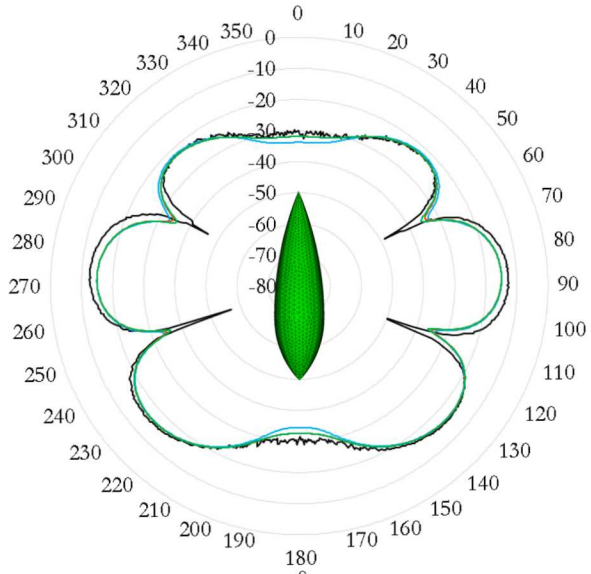

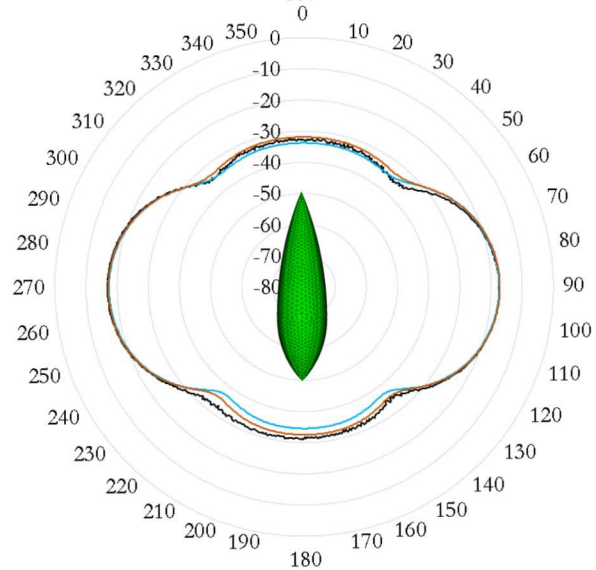

Machine	Waterman
Platform	GPU
EMCC analysis	Gemma
Nodes	
Threads	

Machine	Mutrino
Platform	MIC
EMCC analysis	Gemma
Nodes	1
Threads	

Machine	Mutrino
Platform	CPU
EMCC analysis	Gemma
Nodes	
Threads	